Review on CFD Modelling of Fluidized Bed Combustion Systems based on Biomass and Co-firing

Hemant Kumar[1] · Saroj Kumar Mohapatra[2] · Ravi Inder Singh[3]

Abstract Fluidized bed combustion (FBC) technology has been used effectively for burning conventional fuels long time back. Due to serious environmental concerns and sustainable development approach worldwide, their use in biomass derived furnaces as well in co-firing systems has also proved to be a successful venture since last few years. To analyze, design and optimize the performance of such full scale plants, the need of computational models raised due to time consuming process and high operating costs involved for obtaining data and detailed measurements. In this study an extensive review of CFD applications in FBC systems based on biomass and co-firing has been performed. Basic fluid flow models, different approaches and additional physical and combustion models used in CFD are presented in this paper. At last it is summarized that CFD models provided satisfactory results while validating them in most of the cases. However few challenges are definitely faced for running accurate simulations especially in 3D problems of large scale plants.

Notations

c_p	Specific heat, $Jkg^{-1}K^{-1}$
h_g, h_s	Gas, solid phase enthalpy, Jkg^{-1}
H	Enthalpy, J
I	Radiant intensity
k	Thermal conductivity, $Wm^{-1}K^{-1}$
P_g, P_s	Gas, solid phase pressure, Nm^{-2}
q	Heat flux, W
r, s	Directions
v_g, v_s	Gas, solid phase velocity vector, ms^{-1}
α	Volumetric inter-phase heat-transfer coefficient, $Wm^{-3}K^{-1}$
$\varepsilon_g, \varepsilon_s$	Gas, solid phase volume fraction
μ_g, μ_s	Gas, solid phase shear viscosity, Nsm^{-2}
ρ_g, ρ_s	Gas, solid phase density, kgm^{-3}
σ	Solid-phase shear stress, Nm^{-2}
τ_g, τ_s	Gas, solid phase shear stress, Nm^{-2}
Θ	Granular temperature, ms^{-2}

Abbreviations

BFB	Bubbling fluidized bed
CPP	Captive power plant
FBC	Fluidized bed combustion
LES	Large eddy simulation
NPM	Non-pre mixed
ODE	Ordinary differential equation
PDE	Partial differential equation
PDF	Probability density function
PSH	Primary superheater
RANS	Reynolds average Navier-Stokes
RNG	Re-normalization group
RTE	Radiative transfer equation
TFM	Two fluid model
TPH	Tonnes per hour

✉ Hemant Kumar
   htdhiman@gmail.com; hkumar@pbi.ac.in

[1] Department of Mechanical Engineering, Punjabi University, Patiala 147002, Punjab, India

[2] Department of Mechanical Engineering, Thapar University, Patiala 147004, Punjab, India

[3] Department of Mechanical Engineering, Birla Institute of Technology and Science, Pilani 333031, Rajasthan, India

450

J. Inst. Eng. India Ser. C (August 2018) 99(4):449–474

Introduction

Coal is one of the greatest sources of energy used for power generation across the world, providing almost 40% of the total energy produced [1]. However, coal burning is a major source of CO_2 emission, which adversely affects the climate. Emissions of oxides of nitrogen and sulphur from coal combustion plants have been greatly reduced in the last two decades, but CO_2 emission remains a problem [2]. As a result, combustion techniques based on biomass and co-firing coal with biomass have become increasingly popular [3, 4]. The use of fluidized bed combustion systems has been widely increased for incineration of coal as well biomass since last few years due to their various advantages over conventional fuel firing systems [5–10]. They provide high heat transfer rates, higher combustion efficiency and fuel flexibility in using low grade and low density fuel along with low combustion temperature and less pollutant emissions [11].

FBC system is a complex multiphase flow phenomenon. It comprises of gas phase and emulsion phase. The combustor is divided primarily into three regions; vicinity of bed, that is, dense bed zone, splashing zone just above the dense bed and free board region or lean bed zone [12]. Different homogeneous and heterogeneous reactions taking place amongst gaseous species and fuel particles along with numerous variables such as bed temperature, superficial gas velocity, excess air, particle size distribution, bed and freeboard height and species concentrations make the experimentation in full scale very difficult and expensive. Therefore modelling represents the best method to optimize the performance of these energy conversion units.

In past few years the use of CFD codes is proved to be high potential application in analyzing FBC system [13–17]. The time needed to run theses codes is also reduced due to advanced numerical methods and improved hardware technology. While analyzing the combustion process basic flow models composed of equations of mass, momentum and energy are solved along with submodels of turbulence, chemical species transport and reaction, fuel particle devolatilization, char burnout and radiation energy transport. A CFD code consists of three modules: preprocessor, solver and post-processor.

The great potential of CFD lies in its post-processing which provides qualitative as well quantitative information over the entire domain of the furnace especially in the regions where measurements are difficult or almost impossible to obtain. Another advantage of CFD stands out in using sensitivity analysis that provides the flexibility to change parameters and input values easily which is not easier in laboratory or field experiments. To ensure whether the simulation of domain of interest is adequately completed, the CFD model is validated with experimental data.

The most commonly used CFD codes include Ansys Fluent, CFX, Phoenix, CFD2000, Star CD and AVL fire.

In this paper, an attempt is made to summarize the various CFD applications in the field of FBC systems fuelled by biomass and co-firing of coal and biomass. The achievements of various researchers in terms of temperature profiles, species concentrations of interest, heat fluxes across internal components, char burnout and devolatilization, velocity profiles and particle traces of fuels to study fluid flow and user defined functions (UDF) to study soot deposits and so forth are also discussed along with the challenges faced while running CFD simulations of large scale real plant combustors.

Review of Fluidization

Fluidization is a process in which solids are caused to behave like a fluid by blowing gas or liquid upwards through the solid-filled combustor. Fluidization is widely used in commercial operations; the applications can be roughly divided into two categories, that is, Physical operations, such as transportation, heating, absorption, combustion, mixing of fine powder, etc and chemical operations, such as reactions of gases on solid catalysts and reactions of solids with gases etc [18]. The use of the fluidized bed combustor (FBC) has increased, starting in the twentieth century, spanning from coal combustion and gasification to catalytic reactions. The application field has been recently extended to the incineration of biomass and pre-treated waste, for either power generation or waste disposal. In the next few years, the FBC units are expected to increase further because of the high demand of circulating fluidized beds raised in China [19]. General arrangement of FBC boiler [20] is shown in Fig. 1.

Fluidized bed combustors are being used successfully due to flexible technology evolvement which may use even low quality fuel in terms of its calorific value. These low-heating value fuels can be easily used in FBC due to the high mixing rate of solids and the absence of temperature gradients in the bed. Also the reduction in pollutants emitted with flue gas is one of the most relevant advantages of fluidized bed combustion. The low combustion temperature (700–850°C) guarantees the NO_x abatement while sulphur and halogen capture is achieved by limestone or dolomite injection in the bed [21]. Limestone, within the temperature ranges 700–850°C, not only reacts with SO_2 to form calcium sulphite and calcium sulphate, but also captures hydrogen chloride to form liquid-or solid-phase calcium chloride.

In the field of fluidization the first significant effort was made by Davidson [22] who proposed a simple model for single rising bubbles based on the assumptions that gas
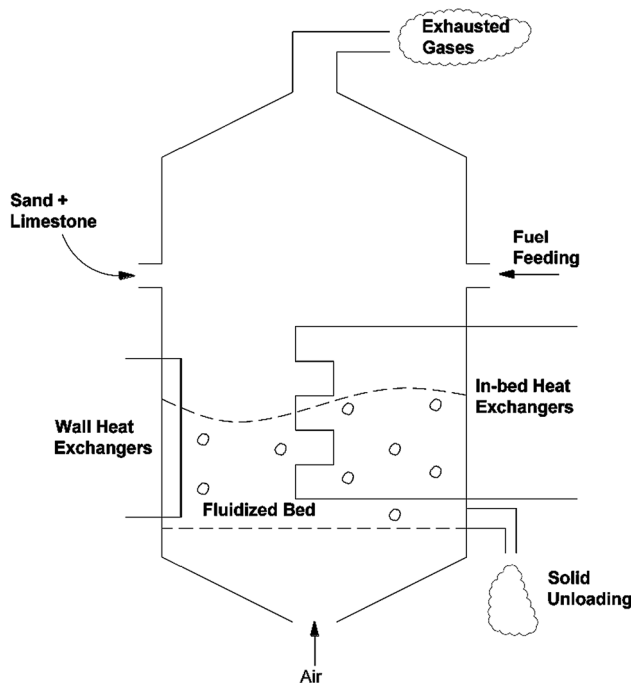
Fig. 1 General arrangement of FBC boiler

bubbles are solid-free and circular in shape, as they rise, particles move aside. The particulate or emulsion behaves like an incompressible fluid through which the gas flows as an incompressible viscous fluid. Pressure inside the bubble remains constant. The most accepted results of this model are the pressure distribution near the bubble region. The pressure in the lower part of the bubble is lower than that of the surrounding bed, whereas in the upper part it is higher. Hence, gas flows into the bubble from bottom and leaves at the top.

Another attempt to understand the behaviour of a bubbling bed was made by Toomey and Johnstone [23], the originators of the two-phase theory of fluidization. The experiments conducted in the field of bubbling beds indicated that all gas needed to fluidize the bed passed through the bed as bubbles and the emulsion phase remained close to minimum fluidizing conditions. In view of that they [23] considered the bubbling bed to be composed of two phases: the bubbling phase and the emulsion phase. The emulsion flow rate is equal to the flow rate for incipient fluidization (U_{mf}) while the bubble phase carries the additional flow of fluidizing fluid ($U - U_{mf}$). It was further observed that the two-phase theory does not explain the evaluation of solids movement in the bed.

Finally a more detailed description of the bubbling bed was proposed by Kunii and Levenspiel [24]. They introduced a new phase called 'cloud', thus their contribution is known as the three-phase theory. This model suggested that if the gas in emulsion phase rises faster than the bubble velocity, then it enters from the bottom of the bubble and

leaves it at the top. This generates an annular ring of gas that circulates within the bubble. On the other hand, if the bubble rises faster than the emulsion, the gas leaving the top of the bubble is swept around and returned to the base of the bubble. The region around the bubble covered by this circulating gas is in the form of cloud. Slow bubbles are usually cloudless whereas, in the case of fast bubbles, cloud cannot be neglected.

The last fluidization model was developed by Werther [25] who was inspired by studies of bed expansion and bubble size distribution. By analogy with gas-liquid reactors, he adopted known mass-transfer phenomena with concentration profiles around the bubbles. The key assumption is concerned with defining a height below which bubble size does not change. Additional hypotheses include the following: the gas flow through the emulsion phase is negligible whereas the one in the bubble phase is a plug flow; the coefficient of mass transfer and the interfacial film between bubble and emulsion are considered independent of the height in the bed.

Fuel particles during combustion inside fluidized bed undergo several phenomena. Firstly, when a fuel particle is injected into a hot fluidized bed it begins to dry. Drying, which usually takes a few seconds, can be followed by shrinkage. Then, further heating at temperature more than 250°C the organic matter of fuel decomposes into volatiles. The process is known as devolatilization that consists of the detachment of the volatile matter from the solid fuel matrix. Average devolatilization time depends on the fuel, on the particle size and on the bed temperature. The residual of devolatilization is made up of char particles which composed of carbon and ash. They burn by reaction with oxygen on the bed. The time in which complete char combustion takes place determines fuel particle residence time in the bed.

Char oxidation may be investigated by different methods, Firstly, by observation of flame formation and extinction [26, 27]. Secondly, by analysis of residual product after combustion [28] and by the measurements of flue gas concentrations [29]. The prediction of char burning time is very useful investigation as it governs the fuel particle residence time in the bed.

Biomass fuels have different chemical and physical composition from those of fossil fuels. They contain higher moisture and volatile content, a lower density and a higher reactivity. Consequently, the behavior of each of the two kinds of fuel in the bed is very different. Coal conversion occurs primarily in the bed, mostly through direct combustion of coarse char particles whereas, for biomass, a large amount of the fixed carbon conversion occurs through the generation of fine particles followed by their post-combustion in the bed, further, a small fraction of the volatile matter burns in the splashing region above the bed [30].

Fludized furnace is divided primarily into three segments according to the different combustion zones: the bed,

452

J. Inst. Eng. India Ser. C (August 2018) 99(4):449–474

the splashing region and the freeboard. The structure of the furnace model is shown in Fig. 2. The fluidized bed is modelled according to the two-phase theory. In the theory the flow rate through the emulsion phase is equal to the flow rate for the minimum fluidization. The flow in excess of minimum fluidization appears as bubbles in the separate bubble phase [31]. The bed is considered isothermal where two phases have uniform temperature. Minimum fluidization velocity is adopted from [32]. An average bubble size is assumed throughout the bed and calculated according to Kato and Wen [33].

It is assumed that fuel is fed above the bed and it spread uniformly and immediately across the cross-section of the bed. In the bed section, according to the two-phase theory, combustion takes place in the emulsion phase. Coarse char and fine char particles are burnt there. In the model the coarse char particles can also burst to the secondary zone of the furnace and drop back into the bed. The fine particles can elutriate out from the furnace [34].

Different combustion systems can be distinguished by the flow conditions in the furnace, thus describing fixed bed combustion, fluidized bed, and entrained flow [35] as shown in Fig. 3.

Biomass Combustion Characteristics

Biomass combustion is a complex process that consists of consecutive homogeneous and heterogeneous reactions. The main process steps are drying, devolatilization,
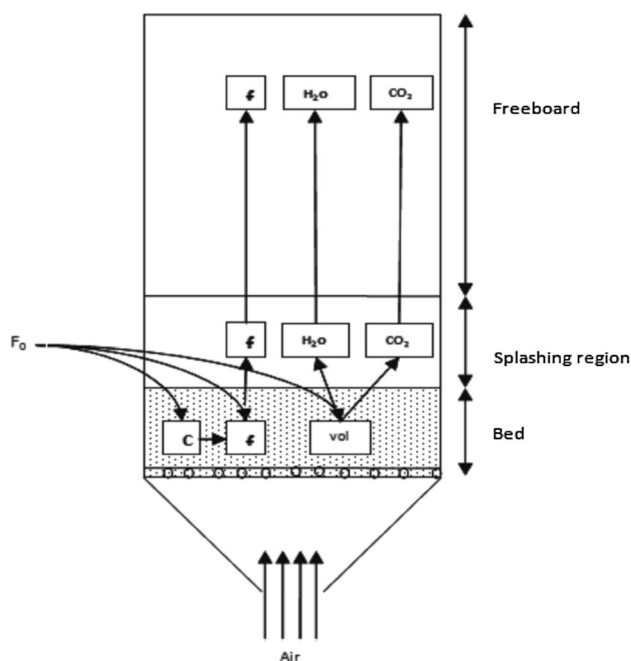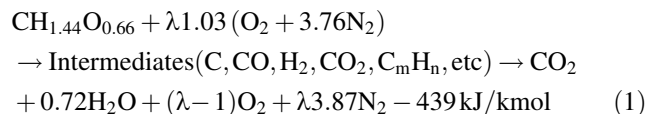

Fig. 2 Structure of the furnace

gasification, char combustion, and gas-phase oxidation. The time used for each process depends on the fuel size, its properties, on temperature, and on combustion conditions. Batch combustion of small particles shows a distinct separation between a volatile and a char combustion phase with time [36, 37] as shown in Fig. 4. For large particles, the phases overlap to a certain extent. The main combustion parameter is the excess air ratio (λ) that describes the ratio between the locally available and the stoichiometric amount of combustion air. For typical biomass, the combustion reaction can be described by the following equation if fuel constituents such as N, K, Cl, etc, are neglected:

$$CH_{1.44}O_{0.66} + \lambda 1.03\,(O_2 + 3.76N_2)$$
$$\rightarrow Intermediates(C, CO, H_2, CO_2, C_mH_n, etc) \rightarrow CO_2$$
$$+ 0.72H_2O + (\lambda - 1)O_2 + \lambda 3.87N_2 - 439\,kJ/kmol \qquad (1)$$

If staged combustion is applied, the excess air may vary in different sections. Two-stage combustion is applied with primary air injection in the fuel bed and secondary air injection in the combustion chamber [37] as shown in Fig. 5. This enables good mixing of combustion air with the combustible gases formed by devolatilization and gasification in the fuel bed. If good mixing is achieved, an operation at low excess air is possible (that is, excess air $\lambda < 1.5$) thus enabling high efficiency with complete burnout of fuel along with little high temperature.

The main needs for complete burnout are temperature, turbulence and time (TTT). The mixing between combustible gases and air can be considered as the most important factor in deciding the burnout quality along with achieving the required temperature (around 850°C) and residence time (around 0.5 s). Sufficient mixing quality can be achieved in fixed bed combustion by the earlier-described two-stage combustion. In fluidized bed, good mixing is achieved in the bed and the freeboard.

For future improvements in furnace design, computational fluid dynamics (CFD) can be applied as a standard tool to calculate flow distributions in furnaces [38] as shown by an example in Fig. 6. Also, the reaction chemistry involved in the gas phase can be implemented in CFD codes [39, 40] However, the heterogeneous reactions during drying, transport, devolatilization and gasification of solid biomass before entering the gas phase combustion need to be considered as well and needs further improvement to enable the application of whole furnace modelling [40–42] as shown in Fig. 7.

Biomass combustion is also used for heat production in small and medium scale units such as wood stoves, log wood boilers, pellet burners, automatic wood chip furnaces, and straw-fired furnaces. These heating systems are in the size range from 0.5 to 5 MW with some applications
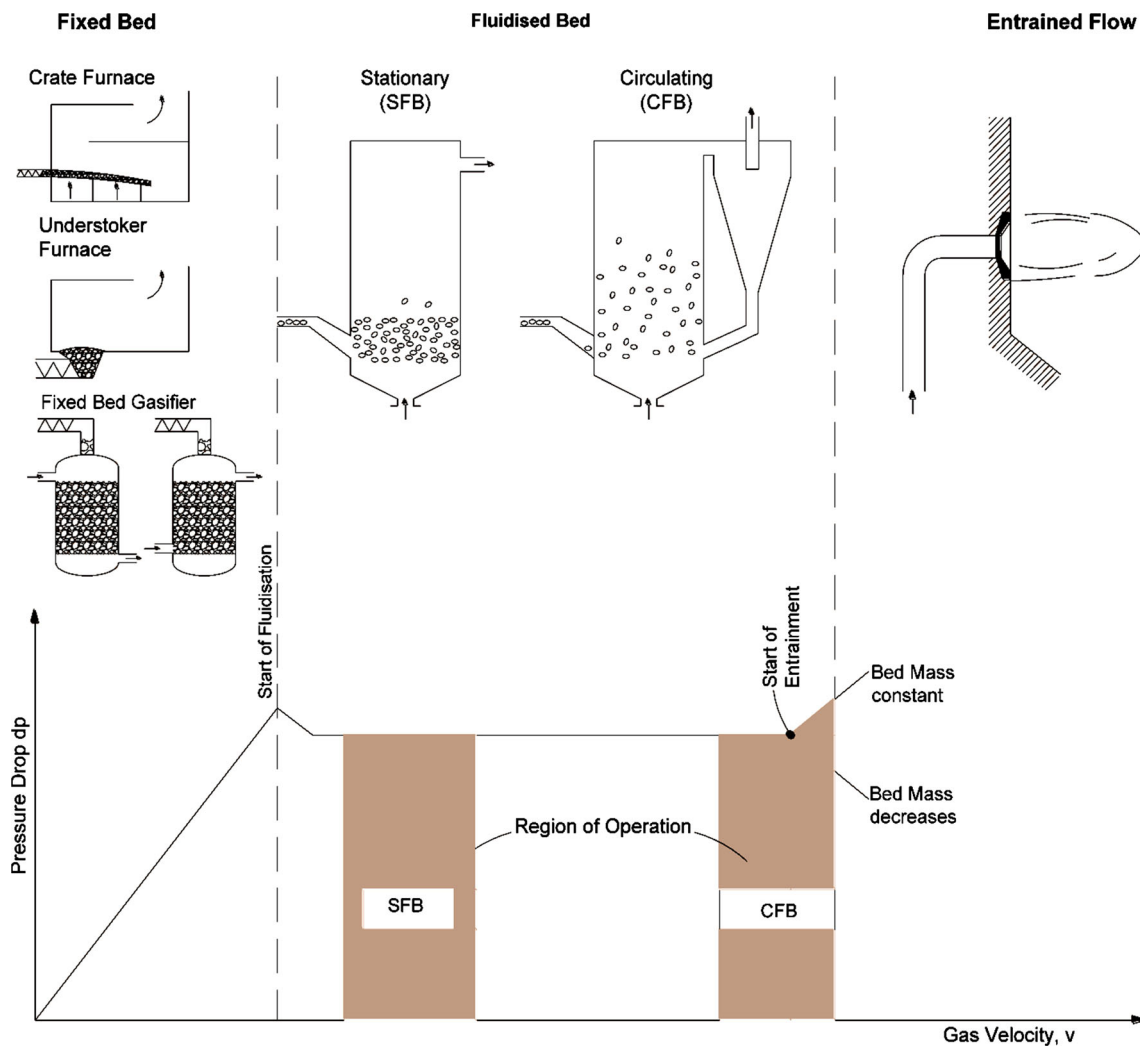
Fig. 3 Furnace types and flow conditions: fixed bed, fluidized bed, and entrained flow
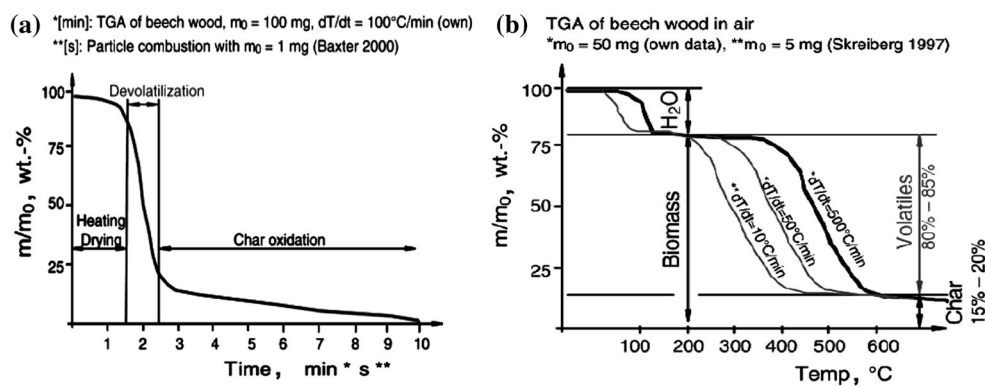

Fig. 4 **a** Mass loss as a function of time, **b** temperature during combustion of wood

up to 50 MW. Combined heat and power production (CHP) with biomass is applied by steam cycles (Rankine cycle) with steam turbines and steam engines and organic Rankine cycles (ORC) with typical power outputs between 0.5 and 10 MW. Fludized bed based co-firing power stations enable the advantages of large size plants (>100 MW), which are however not applicable for a dedicated biomass combustion due to limited local biomass availability.
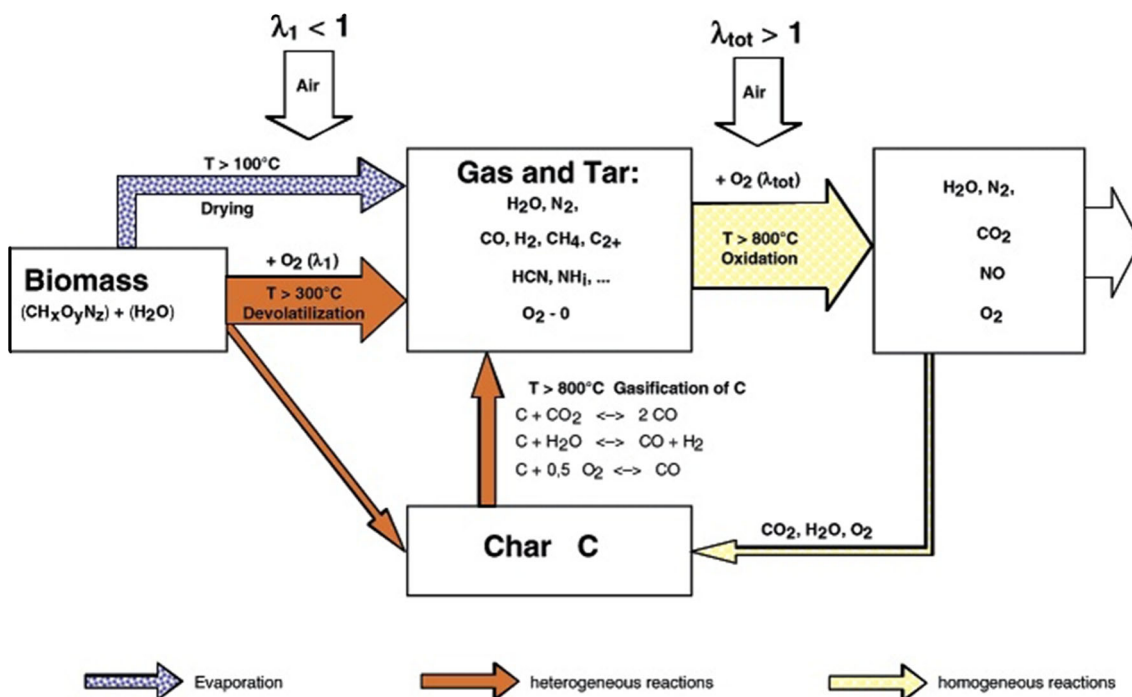
Fig. 5 Main reactions during two-stage combustion of biomass with primary air and secondary air
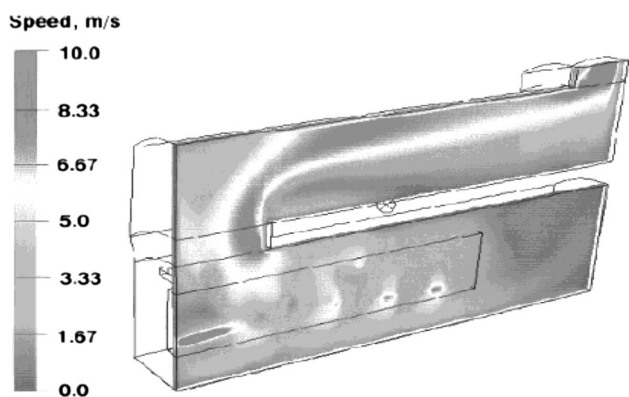

Fig. 6 CFD modelling for optimization of furnace design. The example shows the velocity distribution in the combustion chamber over a grate with secondary air nozzles and post combustion chamber

Overview on Co-combustion

A co-utilization of biomass with other fuels can be advantageous with regard to cost, efficiency, and emissions. Lower specific cost and higher efficiencies of large plants can be utilized for biomass and emissions of SO_x and NO_x can be reduced by co-firing. However, attention must be paid to the increased soot deposition in the boiler tubes and limitations in ash utilization due to constituents in biomass, especially alkali metals that may disable the use of ash in building materials. Due to undesired changes of ash compositions, the share of biomass is usually limited to approximately 10% of the fuel input. Hence, other
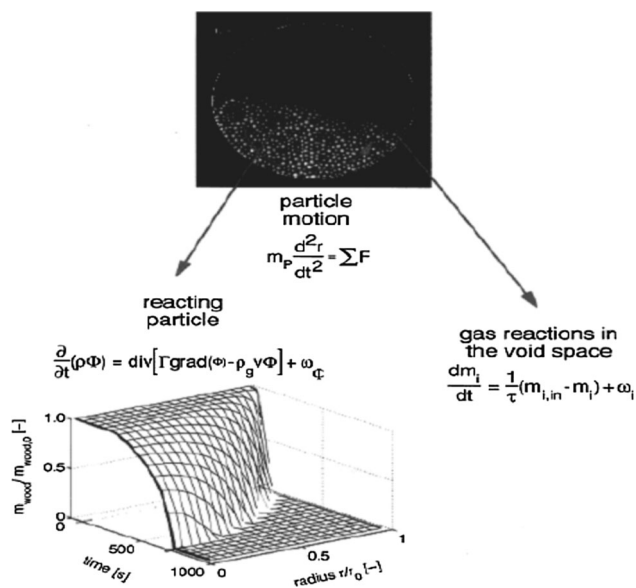

Fig. 7 Basic approach for modelling the solid fuel conversion during combustion of large particles in motion: particle motion, reacting particle, and gas reactions in the void space

opportunities are also of interest and the following three options for co-utilization of biomass with coal are applied:

(a)   Co-combustion or Direct Co-firing: The biomass is directly fed to the boiler furnace (fluidized bed, grate, or pulverized combustion), if needed after physical preprocessing of the biomass such as drying, shredding, and metal removal.

(b) Indirect Co-firing: The biomass is gasified and the product gas is fed to a boiler furnace (a combination of gasification and combustion).

(c) Parallel Combustion: The biomass is burnt in a separate boiler for steam generation. The steam is used in a power plant together with the main fuel. Co-combustion of biomass leads to a substitution of fossil fuels and to a net reduction of CO_2 emissions. In many countries co-firing is the most economic technology to achieve the target of CO_2 reduction and biomass co-firing can therefore be motivated by savings of CO_2 taxes [43].

Co-combustion or Direct Co-firing with Coal

The main application nowadays is direct co-firing in coal-fired power stations. The typical size range is from 50 to 700 MW with a few units between 5 and 50 MW. The co-combustion can be applied in different ways.

(a) The biomass can be burnt in separate wood burners in the boiler. Due to the requirements of pulverized combustion, drying, metal separation, and shredding of the biomass is needed as pretreatment.

(b) As an alternative, the biomass can also be burnt on a separate grate at the bottom of a pulverized coal boiler. The advantage is that costly and energy-consuming fuel pretreatment is not needed, since biomass with high water content and large in size can be burnt.

(c) Further applications of co-combustion with coal are related to BFB, CFB, cyclone, and stoker boilers, which accept a much wider range of fuel size, composition, and moisture content than burners in pulverized coal boilers.

Modelling Approach in CFD

CFD model is based on fundamental assumptions that allow calculation of spatial and temporal variations of temperature and pressure, gas composition, velocity, particle trajectories and so forth. The numerical solution of Navier-Stokes equations in CFD codes usually implies a discretization method, in which a problem involving calculus is transformed into an algebraic problem which can then be solved by computer by using a solution methodology [44]. A discretization technique and a solution methodology constitute the numerical methodology used to solve a heat transfer and fluid flow problem. Among various discretization methods, the most commonly used methods are the Finite difference method (FDM), the finite volume method (FVM) and the Finite element method (FEM) [45]. Different discretization methods are discussed in detail in further section.

With the advent of increased computational capabilities computational fluid dynamics, CFD, is emerging as a very promising new tool in modelling hydrodynamics. While it is now a standard tool for single-phase flows, it is at the development stage for multiphase systems, such as fluidized beds. More attention is required to make CFD suitable for fluidized bed combustor modelling and scale-up. Two different approaches have been earlier attempted to apply CFD modelling to gas-solid fluidized beds: a discrete method based on molecular dynamics (Lagrangian model); and a continuous approach based on continuum mechanics, treating the two phases as continuous phase (multifluid or Eulerian-Eulerian model). These two approaches have been compared by Gera, et al [46].

The theory behind the Eulerian approach is based on the macroscopic balance equations of mass, momentum, and energy for both phases. Eulerian models treat the particle and the gas phase as two interpenetrating continuous media [47] and assume that both phases occupy every element of the computational domain. The gas phase is called the primary or continuous phase and the solid phase is called the granular or dispersed phase. Both phases are represented by their volume fractions and are linked through the drag force in the momentum equation as given by Wen and Yu's [48] correlation for a dilute system, Ergun's [49] correlation for a dense system, and Gidaspow, et al [50] which is a combination of both correlations for fluctuating systems. An averaging technique is adopted for the field variables such as the gas and solid velocities, solid volume fraction, and solid granular temperature. The kinetic theory for granular flow (KTGF, discussed later) is used to derive constitutive relations based on empirical information to describe the interparticle interaction and to close the set of conservation equations.

Eulerian-Eulerian modelling approach treats the fluid and solid phases as interpenetrating continuum phases and is the most commonly used approach for fluidized bed simulations [51]. In this scheme, collection of particles is modelled using continuous medium mechanics. The solid particles are generally considered to be identical having same diameter and density. The general idea in constructing the multifluid model is to treat each phase as an interpenetrating continuum, and therefore to formulate integral balances of continuity, momentum and energy equations for both phases, with appropriate boundary conditions for phase interfaces. Since the resultant continuum approximation for the solid phase has no equation of state and lacks variables such as viscosity and normal stress [51], certain averaging techniques and assumptions are required to obtain a momentum balance for the solids phase. CFD simulations for the heat transfer in bubbling fluidized beds for Eulerian-Eulerian model are also reported by Kuipers [52] and Schmidt and Renz [53] for 2D and Gustavasson and Almstedt [54] for 3D.

Averaging theorems are applied to construct a continuum for each phase in order to describe the Eulerian

approach of single-phase flow to be extended to the multiphase flow. Although the transport coefficients of the gas phase may be represented for a single-phase flow with certain modifications, the transport coefficients of the solid phases must also be accounted for gas-particle interactions and particle-particle collisions. The interphase momentum transfer between gas and solid phases is one of the dominant forces in the gas- and solid phase momentum balances. This momentum exchange is represented by a drag force. The drag force on a single particle in a fluid has been well studied and empirically correlated by Clift, et al [55] and Bird, et al [56], for a wide range of particle Reynolds numbers. However, when a single particle moves in a dispersed two-phase mixture, the drag is affected by the presence of other particles. Numerous correlations for calculating the momentum exchange coefficient of gas-solid systems have been reported in the literature, including those of Syamlal and O'Brien [57], Gidaspow [58] and Wen and Yu [59].

On the other hand, Lagrangian models, or discrete particle models, are derived by applying Newton's law of motion for the particulate phase. This approach leads to the ability of computing the trajectory (path) and motion of individual particles. The interactions between the particles are described by either a potential force (soft particle dynamics) [60] or by collision dynamics (hard particle dynamics) [61]. In this approach, the fluid phase is treated separately by solving a set of time-averaged Navier-Stokes equations, whereas the dispersed phase is solved by tracking a large number of particles, bubbles, or droplets through the calculated flow field.

In the Lagrangian model of two-phase flow, the Newtonian equations of motion for each individual particle are solved by including the effects of particle collisions and forces acting on the particles by the gas. Particle-particle collisions are modelled by the hard sphere or soft sphere approach [62]. The discrete particle model, DPM, is one of the trajectory models, which can calculate the particle velocity and the corresponding particle trajectory due to multi body collisions [63]. Trajectory models are applied to multiphase flows for dilute systems where a continuum model for the particle is not appropriate. Though models based on a DPM allow the effects of various particle properties on the motion of fluid to be studied, it is computationally intensive. Due to computational limitations, the Eulerian-Lagrangian model is normally limited to a relatively small numbers of particles. Therefore, the multi fluid model is the preferred choice for simulating macroscopic hydrodynamics. Figure 8 shows the multi level modelling scheme based upon the information gathered from different simulations [64].

Furthermore, using the Lagrangian approach, the dispersed phase can exchange mass, momentum, and energy
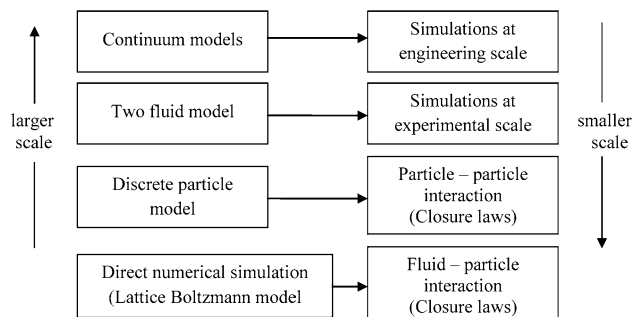
Fig. 8 Multi-level modelling scheme based upon Hoef, et al

with the fluid phase through the conservation equations. These equations also account for the changes in volume fraction of each phase. As each individual particle moves through the flow field, its trajectory, mass, and heat transfer calculations are obtained from a force balance along with local conditions of the continuous phase. Thus, external forces acting on the solid particle such as aerodynamic, gravitational, buoyancy, and contact due to collisions between the particles themselves and between the particles and the side wall of the furnace can be calculated simultaneously with the particle motion using local parameters of gas and solids. Although the Eulerian momentum equation can be derived from its Lagrangian equivalent by averaging over the particle phase, each model has its advantages and disadvantages depending on the objective of the study and the type of system used. By the use of earlier definitions of two approaches, the merits and shortcomings of each formulation are discussed.

Merits and Demerits of Each Approach

Some of the advantages and disadvantages of the Eulerian and Lagrangian formulations are discussed in this section. Examples of their use for actual physical systems are also provided for easier understanding of the subject and to guide the researchers and academicians for the appropriate formulation and implementation to their problems at hand.

Lagrangian description is more suitable for particle-laden flows having low concentration of particles with volume fraction up to the order of 10^{-2} or less. This characteristic of particles density allows the tracking of particles trajectories (computed by applying Newton's second law of motion to each particle) at different locations in the computational domain because computational effort can be handled with the available computing facility. This is the main distinctive advantage of this technique over the Eulerian formulation. This in turn provides the opportunity to evaluate interactions between particles, fluids, and boundaries using local flow parameters and gas properties, which is difficult to achieve using a steady-state model. The total numbers of particles are traced from a

computational point of view and modelling particle-particle and particle-wall interactions can be achieved with a great success. These models can apply any interparticle forces (cohesive or vander Waals) for any particle shape and size. Finally, Lagrangian models are less prone to numerical diffusion errors, more stable for flows with large particle velocity gradients, and readily applied to poly dispersed particle systems [65]. Therefore, Lagrangian models are suited to study the phenomena of segregation, fragmentation, or agglomeration [66].

Some of the drawbacks of the Lagrangian approach are the large memory requirements and long computation time taken by the iterative process to converge. In addition, Lagrangian models are only applicable to small size systems as in the case of dilute systems; thus, in concentrated systems with significant particle-fluid and particle-particle interaction, model formulations are not suitable due to lack of fundamental understanding of the interaction and the reliance on empirical information. Finally, Lagrangian models do not seem to be applicable in systems where lubrication forces (shear and pressure forces exerted on the fluid-particle surface due to viscous shearing of fluid layers with each other) are considered.

On the other hand, the Eulerian approach is more appropriate for modelling particle suspension, circulating fluidized beds, risers, and bubble columns. Therefore, it enables the computation of dense phase systems. In brief, the Eulerian description is suitable for high concentration of the particle phase. By using averaging procedures, it offers a formal methodology for developing numerical solutions of direct and indirect particle interaction and fluid turbulence.

One of the shortcomings of the Eulerian models is the assumption of monosized particles. Another shortcoming is the average technique used by the Eulerian models to represent field variables such as particle volume fraction, momentum, rotation, and orientation. Hence, details of the individual collisions are averaged and removed from the field equations. The most commonly adopted Eulerian models have problems close to the wall region where particles change directions due to interaction with the wall materials. An example of a limitation of Eulerian model in comparison to the Lagrangian model is in the description of erosion pattern provided by Johansen and Laux [66].

In conclusion, both models inherit deficiencies due to insufficient understanding of the complex particle-particle and particle-fluid interactions that develop in turbulent flow and the mathematical complexities of representing these phenomena. However, the application of both the approaches for the design and optimization of various units such as dryers, chemical reactors, and fluidized beds cannot be denied.

Discretization Methods

As discussed earlier to solve different governing equations used to represent multiphase flow systems they need to be shaped in a form compatible with numerical algorithms. Note that the nature of the governing equations is either nonlinear ordinary differential equations (ODE) or partial differential equations (PDE) depending on the formulation used and the assumptions implemented for their formulation. Because no direct methods are available for solving these types of equations, an alternative (approximate solutions) is to transform them into simpler forms that are less mathematically and numerically complex. This can be achieved using one of the commonly used discretization techniques: finite difference, finite volume, and finite element.

A finite difference discretization (FDD) is based upon the differential form of the PDE to be solved. Each derivative is replaced with an approximate difference formula (backward, central, and forward difference) that can generally be derived from a Taylor series expansion. The computational domain is usually divided into hexahedral cells (grid), and the solution is then obtained at each nodal point. The FDD is easier to understand when the physical grid is Cartesian, but through the use of curvilinear transforms, the method can be extended to domains that are not easily represented by these elements. The discretization technique results in a system of equations for the solution variables at nodal points [67].

A finite volume discretization (FVD) is based upon dividing the computational domain into small geometrical volumes or cells that numerically define the region of interest. The integral form of the conservation equations of mass, momentum, and energy are solved for each control volume in addition to constitutive equations describing turbulence, chemical reactions, transport of particles, and radiation. Consequently, the quality of the solution in the computational domain depends to a large extent on the size, shape, and placement of the control volumes. Other factors that are equally important and also contribute to the quality of the solution are the boundary conditions at the inlet and outlet of the domain as well as the wall boundary conditions [68].

Finally, a finite element discretization (FED) is based upon a piecewise representation of the solution in terms of specified basis functions. The FED uses a more general approach than the FDD and FVD, both of which are types of the FED. It is suitably used for large domains and complex geometrical problems. With the FED technique, the computational domain is divided into smaller domains (thus finite elements) and the solution in each element is constructed from the basis functions. The actual equations that are solved are obtained from the conservation

equations and the field variables are written in terms of the basic functions and the equation is multiplied by appropriate test functions and then integrated over an element [69, 70].

The major advantage of the FVD over FDD is its ability to solve the solution variables without the need for structured mesh, thus the effort to convert the given mesh into structured grid internally is not required. As with FDD, the resulting approximate solution is discrete, but the variables are typically placed at cell centers rather than at nodal points. In cases where field variables are to be estimated at non storage locations, an interpolation technique is followed.

Comparison of these three methods is difficult, primarily due to the many variations. Both FVD and FDD provide discrete solutions, whereas FED provides a continuous solution. Both FVD and FDD are generally considered easier to program than FED because the latter approximates continuous quantities as a set of quantities at discrete points which are mathematically challenging, whereas the FVD calculates the values of the conserved variables averaged across the volume using averaging techniques, and the FDD extrapolates a finite amount of data to find a general term. The decision regarding which method to use should be based on a fundamental understanding of the physical model under consideration along with a solid understanding of the capabilities of each of the three mentioned computational techniques.

Mathematical Description of CFD Models

The governing equations used during the modelling study in FLUENT consisted of mathematical models of the gas phase and reactive chemistry. Prediction of the isothermal flow field in the computational grid is done through the solution of the equations for the conservation of mass and momentum and interphase heat exchange through energy balance equations as follows:

Mass Balance Equations

Gas phase

$$\frac{\partial}{\partial t}(\varepsilon_g \rho_g) + \nabla(\varepsilon_g \rho_g v_g) = 0 \tag{2}$$

Solid phase

$$\frac{\partial}{\partial t}(\varepsilon_s \rho_s) + \nabla(\varepsilon_s \rho_s v_s) = 0 \tag{3}$$

where ε_g and ε_s are gas and solid phase volume fractions; ρ_g and ρ_s are gas and solid phase densities (kgm^{-3}) and v_g and v_s are gas and solid phase velocity vectors (ms^{-1}), respectively.

Momentum Balance Equations

Gas phase

$$\frac{\partial}{\partial t}(\varepsilon_g \rho_g v_g) + \nabla(\varepsilon_g \rho_g v_g) = \nabla\tau_g - \varepsilon_g \nabla P_g - \varepsilon_g \rho_g g - \beta(v_g - v_s) \tag{4}$$

Solid phase

$$\frac{\partial}{\partial t}(\varepsilon_s \rho_s v_s) + \nabla(\varepsilon_s \rho_s v_s) = \nabla\tau_s - \varepsilon_s \nabla P_s - \varepsilon_s \rho_s g - \beta(v_s - v_g) \tag{5}$$

where P_g and P_s are gas and solid phase pressures (Nm^{-2}); β is inter-phase drag coefficient and τ_g and τ_s are gas and solid phase shear stresses (Nm^{-2}), respectively.

Energy Balance Equations

Gas phase

$$\frac{\partial}{\partial t}(\varepsilon_g \rho_g h_g) + \nabla(\varepsilon_g \rho_g h_g v_g) = -\nabla\varepsilon_g q_g + \alpha(T_g - T_s) + \tau_g \nabla v_g + \varepsilon_g\left(\frac{\partial}{\partial t}p + v_g \nabla p\right) \tag{6}$$

Solid phase

$$\frac{\partial}{\partial t}(\varepsilon_s \rho_s h_s) + \nabla(\varepsilon_s \rho_s h_s v_s) = -\nabla\varepsilon_s q_s + \alpha(T_g - T_s) + \tau_s \nabla v_s + \varepsilon_s\left(\frac{\partial}{\partial t}p + v_s \nabla p\right) \tag{7}$$

$$h_i = \int_{Tref}^{T} c_{p,i}dT_i \quad \text{and} \quad q_i = -k_i \nabla T_i \tag{8}$$

Devolatilization Submodels

The devolatilization process begins when the biomass temperature reaches a critical level. Many biomass devolatilization models have been developed and several reviews of these models have been made [71–74]. One-step global mechanisms and semi-global multi-step mechanisms can be basically distinguished. The simplified approaches define devolatilization rates with single or two-step Arrhenius reaction schemes. The one-step global mechanisms can be shown as

$$Biomass \xrightarrow{k} Volatiles + Char \text{ or } Biomass \xrightarrow{k} Tar(Bio-oil) + Gases + Char \tag{9}$$
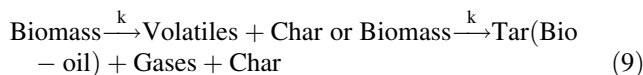
The reaction kinetic rate (k) is expressed in single-step Arrhenius fashion as $k = A \exp(-E_a/RT)$ and the devolatilization rate is

$$-\frac{dm_p}{dt} = k[m_p - (1 - f_{v,0})m_{p,0}] \tag{10}$$

where m_p is the biomass particle mass; $m_{p,0}$ is the initial particle mass; and $f_{v,0}$ is the initial volatile fraction [75].

For two-step Arrhenius reaction schemes, the kinetic devolatilization rate expressions of the form proposed by Kobayashi [76] are

$$k_1 = A_1 \exp(-E_a/RT) \tag{11}$$
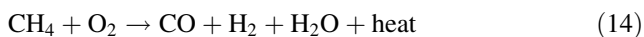
$$k_2 = A_2 \exp(-E_a/RT) \tag{12}$$

where k_1 and k_2 are competing rates that may control the devolatilization over different temperature ranges. The two kinetic rates are weighted to yield an expression for the devolatilization as:

$$\frac{m_v(t)}{(1-f_{w,0})m_{p,0}-m_a} = \int_0^t (a_1k_1 + a_2k_2) \exp\left(-\int_0^t (k_1+k_2)dt\right)dt \tag{13}$$

where $m_v(t)$ is the volatile yield up to time t; $m_{p,0}$ is the initial particle mass at injection; α_1 and α_2 are yield factors; and m_a is ash content in the particle [76].

Homogenous Gas-Phase Reactions Submodels

The solid fuel devolatilization and cracking gas species will react with supplied oxidizer and with each other such as water-gas shift reaction. The heat generated by exothermic reactions is important for the release of volatiles and ignition of char. The general homogenous reactions taking place are as follows.

$$CH_4 + O_2 \rightarrow CO + H_2 + H_2O + \text{heat} \tag{14}$$

$$CO + H_2O \leftrightarrow CO_2 + H_2 \tag{15}$$

$$O_2 + 2H_2 \leftrightarrow 2H_2O \tag{16}$$

Heterogeneous Reaction Submodels

Char is the solid devolatilization residue. Heterogeneous reactions of char with the gas species is complex process which involve the balancing rate of mass diffusion of the oxidizing chemical species to the surface of fuel particle with the surface reaction of these species with the char. The overall rate of a char particle is determined by the oxygen diffusion to the particle surface and the rate of surface reaction, which depend on the temperature and composition of the gaseous environment and the size, porosity and temperature of the particle. The commonly simplified reactions models which consider the following overall reactions:

$$C_{char} + {}^1\!/_2 O_2 \rightarrow CO + \text{heat} \tag{17}$$

$$C_{char} + CO_2 \rightarrow 2CO \tag{18}$$

$$C_{char} + H_2O \rightarrow CO + H_2 \tag{19}$$

The literature that reviewed the char surface reactions and the kinetic relationship can be found from [77, 78].

Additional Physical Submodels

Navier-Stokes equations describing basic flow equations like mass, momentum and energy are not found sufficient to model combustion and gasification of fuel in fluidized beds. Additional physical models are also needed to represent all physical processes. These models include turbulence models, heat transfer with radiation, mass transfer and diffusion etc. In this study commonly used models are explained, however more detailed and advanced physical models may be referred from Bakul, et al [79].

Turbulence Model

Turbulent flows are characterized by fluctuating velocity fields. These fluctuations mix transported quantities such as momentum, energy, and species concentration, and cause the transported quantities to fluctuate as well. Since these fluctuations are usually of small scale and high frequency, thus they are computationally very expensive to simulate directly in practical engineering calculations. So these governing equations can be time-averaged, ensemble-averaged, or otherwise manipulated to remove the small scales, resulting in a modified set of equations that are computationally less expensive to solve. However, the modified equations contain additional unknown variables, and turbulence models are needed to determine these variables. The choice of turbulence model will depend on considerations such as the actual physics applied in the flow, the level of accuracy required, the available computational space, and the amount of time available for the simulation.

Turbulent flows are characterized by fluctuating velocity fields primarily due to the complex geometry and/or high flow rates. Turbulence affects the heat and mass transfer and plays an essential role in some processes such as biomass gasification and non-premixed combustion in fluidized bed furnaces. The Navier-Stokes equations can be solved directly for laminar flows, but for turbulent flows the direct numerical simulation (DNS) with full solution of the transport equations at all length and time scales is too computationally expensive since the fluctuations can be of small scale and high frequency. The DNS is only restricted to simple turbulent flows with low to moderate Reynolds numbers. In the cases of high Reynolds number flows in complex geometries, a complete time-dependent solution of the Navier-Stokes equations is quite difficult in present computational capabilities. Hence, turbulence models are required to account for the effects of turbulence rather than

simulate it directly in practical engineering applications. Two alternative methods are employed to transform the Navier-Stokes equations so that the small eddies do not have to be directly simulated: Reynolds averaging and filtering. Both methods introduce additional terms in the governing equations that must be modelled for turbulence closure.

RANS-based Models

The Reynolds-averaged Navier-Stokes (RANS) equations represent transport equations for the mean flow quantities only, with all the scales of turbulence being modelled. The RANS models are developed by dividing the instantaneous properties in the conservation equations into mean and fluctuating components, as shown as:

$$\phi = \bar{\phi} + \phi' \tag{20}$$

The averaging of the flow field variables is used to account for the effects of density fluctuations due to turbulence. This technique brings Reynolds stress terms in the time-averaged conservation equations and modelled for turbulence closure. The Reynolds-averaged approach is generally adopted for practical engineering calculations.

Most common RANS models employ the Boussinesq hypothesis (eddy viscosity concept, EDC) to model the Reynolds stresses terms. The hypothesis states that an increase in turbulence can be represented by an increase in effective fluid viscosity, and that the Reynolds stresses are proportional to the mean velocity gradients through this viscosity. Models based on this hypothesis include Spalart-Allmaras, standard k-ε, RNG k-ε, Realizable k-ε, k-ω and its variants. The Reynolds stress model (RSM) closes the Reynolds-averaged Navier-Stokes equations by solving transport equations for the Reynolds stresses directly, together with an equation for the dissipation rate. The details of earlier models and RSM could be referred from Bakul, et al [79]. In majority of works standard k-ε [80] is used in combustion and gasification of fuels in fluidized beds.

$$\frac{\partial}{\partial t}\left(\alpha_g \rho_g k_g\right) + \nabla\left(\alpha_g \rho_g \vec{v}_g k_g\right) = \nabla\left(\alpha_g \frac{u_{t,g}}{\sigma_k} \nabla k_g\right)$$
$$+ \alpha_g G_{k,g} - \alpha_g \rho_g \varepsilon_g + \alpha_g \rho_g \prod_{k,g} \tag{21}$$

$$\frac{\partial}{\partial t}\left(\alpha_g \rho_g \varepsilon_g\right) + \nabla\left(\alpha_g \rho_g \vec{v}_g \varepsilon_g\right) = \nabla\left(\alpha_g \frac{u_{t,g}}{\sigma_e} \nabla k_g\right)$$
$$+ \alpha_g \frac{\varepsilon_g}{k_g}\left(C_{1e}C_{k,g} - C_{2e}\rho_g \varepsilon_g\right) + \alpha_g \rho_g \prod_{e,g} \tag{22}$$

where $\prod_{k,g}$ and $\prod_{e,g}$ are influence of the dispersed phase on the continuous phase, C_{1e}, C_{2e}, $C_{k,g}$, σ_k and σ_e are model constants and $G_{k,g}$ is the production of turbulent linetic energy.

LES Models

Large eddy simulation (LES) solves 'filtered' transport equations by permitting direct simulation of large scale turbulent eddies. Filtering removes eddies that are smaller than the filter size, which is usually taken as the mesh size. LES provides an accurate solution to the large scale eddies instead of DNS while the smaller eddies below the filter size are modelled. This is because the large turbulent eddies are highly anisotropic and dependent on both the mean velocity gradients and the flow region geometries, while smaller eddies possess length scales determined by the fluid viscosity and are consequently isotropic at high Reynolds numbers. LES offers an alternative method of reducing the errors caused by RANS and providing a more accurate technique for turbulence simulation. However, application of LES to biomass industrial engineering is still in its developing stage due to its computational requirements.

Radiation Modelling

The radiative transfer equation (RTE) for an absorbing, emitting, and scattering medium at position in the direction can be written as follows:

$$\frac{dI\left(\vec{r}, \vec{s}\right)}{ds} + (a + \sigma_s)I\left(\vec{r}, \vec{s}\right)$$
$$= an^2 \frac{\sigma T^4}{\pi} + \frac{\sigma_s}{4\pi} \int_0^{4\pi} I\left(\vec{r}, \vec{s}\right)\Theta\left(\vec{r}, \vec{s}\right)d\Omega' \tag{23}$$

A semi-transparent medium is considered and the refractive index is equal to unity.

The following models are applicable.

(a) Discrete ordinates model;
(b) P-1 model;
(c) Rosseland model; and
(d) Discrete transfer radiation model.

The details of all these models should be referred from Bakul, et al [79]. The earlier models could be used in combustion and gasification process based on optical thickness aL where a is constant and L is an appropriate length scale. The P-1 and Rosseland models are useful when aL ≫ 1. The P-1 model should typically be used for optical thicknesses large than 1. The Rosseland model is computationally cheaper and more efficient but should only be used for optical thicknesses larger than 3. The discrete ordinates model (DOM) works across the range of optical thicknesses, but is substantially more computationally expensive than the Rosseland model [75]. The discrete transfer radiation model is also used rarely as being computationally expensive.

Mixture Fraction Model

Non premixed combustion model (NPM) has been applied to simulate combustion in which mixture fraction/probability density function (PDF) approach is used. This approach involves the solution of transport equations for one or two conserved scalars (the mixture fractions). Through this approach, instead of solving the transport equations for individual species, the component concentrations of species of interest are derived from the predicted mixture fraction. Therefore, the usually unknown reaction mechanism is not explicitly solved but it is treated using certain system chemistry calculations (for example, equilibrium assumption and non-equilibrium chemistry). Physical properties of chemical species and equilibrium data are retrieved from the chemical database while the interaction of turbulence and chemistry is obtained with a probability density function or PDF.

The PDF modelling approach is considered computationally efficient method because a large number of species transport equations need not required to be unnecessarily solved. The basis of the mixture fraction approach is that, the thermo-chemical state of the fluid is related to a conserved scalar quantity known as the mixture fraction, f. Being a conserved scalar quantity, the value of f at each point in the flow domain is computed in FLUENT through the solution of the conservation equation for mean value of f in the turbulent flow field using following relation:

$$\frac{\partial}{\partial x_i}\left(\rho u_i \bar{f}\right) = \frac{\partial}{\partial x_i}\left(\frac{\mu_t}{\sigma_t}\frac{\partial \bar{f}}{\partial x_i}\right) + S_m \tag{24}$$

where u_i is fluid velocity at any point in turbulent field; $\bar{f}$ is mean value of mixture fraction; μ_t is turbulent viscosity; and σ_t is a constant. S_m represents the transfer of mass from reacting particles into the gas phase. In addition to earlier equation, a conservation equation for the mixture fraction variance, $\overline{f'^2}$ is also solved:

$$\frac{\partial}{\partial x_i}\left(\rho u_i \overline{f'^2}\right) = \frac{\partial}{\partial x_i}\left(\frac{\mu_t}{\sigma_t}\frac{\partial \overline{f'^2}}{\partial x_i}\right) + C_g \mu_t \left(\frac{\partial \bar{f}}{\partial x_i}\right)^2 - C_d \rho \frac{\varepsilon}{k}\overline{f'^2} \tag{25}$$

where the constants σ_t, C_g and C_d are given the default values by solver which is FLUENT itself. The mixture fraction variance is used to describe the turbulence-chemistry interaction. Calculation of a single conserved scalar field, f also derives of other important scalars which are density and temperature without the need to solve their respective transport equations. Provided the description of the reacting system chemistry, the mixture fraction value at each point in the flow field can be used to compute the instantaneous values of these scalars. If a secondary stream is included in the system, then the instantaneous values will depend on fuel mixture fraction f_{fuel}, the secondary partial fraction p_{sec}, and time averaged enthalpy H^*

$$\Phi_i = \Phi_i(f_{fuel}, p_{sec}, H^*) \tag{26}$$

where Φ_i represents the instantaneous species concentration and H^* is given by:

$$H^* = \sum_i m_i H_i = \sum_i m_i \left(\int_{T_{ref_i}}^{T} c_{p,i}dT + h_i^o(T_{ref_i})\right) \tag{27}$$

where H_i represents instantaneous enthalpy.

Discrete Phase Model (DPM)/Equation of Motion of a Particle

FLUENT predicts the trajectory of a discrete phase particle by integrating the force balance on the particle, which is written in a Lagrangian reference frame. This force balance equates the particle inertia with the forces acting on the particle, and can be written (for the x direction in Cartesian coordinates) as

$$\frac{du_p}{dt} = F_D(u - u_p) + \frac{g_x(\rho_p - \rho)}{\rho_p} \tag{28}$$

where $F_D(u - u_p)$ is the drag force per unit particle mass and

$$F_D = \frac{18\mu}{\rho_p D_p^2}\frac{C_D Re}{24} \tag{29}$$

Here, u is the fluid phase velocity; u_p is the particle velocity; μ is the molecular viscosity of the fluid; ρ is the fluid density; ρ_p is the density of the particle; and D_p is the particle diameter. R_e is the relative Reynolds number, which is defined as

$$Re = \frac{\rho D_p |u_p - u|}{\mu} \tag{30}$$

The drag coefficient, C_D can be taken from either

$$C_D = a_1 + \frac{a_2}{Re} + \frac{a_3}{Re^2} \tag{31}$$

where a's are constants that apply for smooth spherical particles over several ranges of Re given by Morsi and Alexander [81] or

$$C_D = \frac{24}{Re}\left(1 + b_1 Re^{b_2}\right)\frac{b_3 Re}{b_4 + Re} \tag{32}$$

where

$$b_1\ \ 2.3288 - 6.4581\phi + 2.4486\phi^2 \tag{33}$$

$$b_2\ \ 0.0964 + 0.5565\phi \tag{34}$$

$$b_3\ \ 4.905 - 13.8944\phi + 18.4222\phi^2 - 10.2599\phi^3 \tag{35}$$

$$b_4\ \ 1.4681 + 12.2584\phi - 20.7322\phi^2 + 15.8855\phi^3 \tag{36}$$

Table 1 CFD applications in biomass combustion

Application	Code	Dim	Aim/outcome	Turb. model	Extra model	Agreement with exp.	Authors
Bagasse fired boilers [83]	Furnace	3D	Tube erosion; heat transfer; Airheater corrosion; Swirl burner	Std k-ε	Lagrangian porous	Acceptable	Dixon, T. F.
Straw-fired grate boiler [84–87]	CFX	3D	To provide insight into the boilers; heat transfer predictions; To predict ash deposition	RNG k-ε	DTRM	Good	Kær, S. K.
Combustion furnace [88]	Fluent	3D	Particle tracks, temperature contours	Std k-ε	Lagrangian DOM	NA	Shanmukha radhya, K. S.
Waste rotary kiln incinerator [89]	Fluent	3D	To describe the processes occurring within the gaseous phase of the kiln and of the post combustion chamber	Std k-ε	P1	NA	Marias, F.
Bagasse fired furnaces [90]	Fluent	3D	To gain insight into the effect of moisture on the flame front.	k-ε	Lagrangian P1	NA	Shanmukha radhya, K. S.
Tube stove [91]	CFX TASCf low	3D	To understand the aerothermo-chemical behaviour of the stove operation in combustion and gasification modes	NA	c-phase	Excellent	Dixit, C. S. B.
Waste-to energy plant [92]	Fluent FLIC		To maximize the energy recovery efficiency of waste-to-energy plants	k-ω	DOM	NA	Goddar, C. D.

Dim dimension, *Turb* turbulence, *Std* standard, *DOM* discrete ordinates model (radiation), *DTRM* discrete transfer radiation model, *P1* P1 radiation model, *Exp* experiment

which is taken from Haider and Levenspiel [82] for non spherical particles. The shape factor, ϕ, is defined as ϕ = s/S, where s is the surface area of a sphere having the same volume as the particle, and S is the actual surface area of the particle.

The trajectory equations were solved by stepwise integration over discrete time steps. Integration in time of Eq. (28) yielded the velocity of the particle at each point along the trajectory, with the trajectory itself predicted by

$$\frac{dx}{dt} = u_p, \frac{dy}{dt} = v_p, \frac{dz}{dt} = w_p \qquad (37)$$

The particle phase was assumed to be sufficiently dilute, thus rendering negligible effects on the continuous phase.

Application of CFD in Biomass Combustion or Co-firing Boilers and Furnaces

Large number of application of CFD models were found in power station boilers and furnaces. Many systems initially made for using coal combustion have been modified to apply to biomass combustion or cofiring. Tables 1 and 2 summarize the recent studies that apply CFD to simulate biomass combustion and co-firing boilers and furnaces. CFD modelling has established itself as a critical tool for the development of new ideas and advanced technologies. It is capable of predicting qualitative information and quantitative information within sufficient accuracy to justify engineering design changes on experimental setups as well commercial power plants.

Dixon, et al [83] summarized the CFD applications on bagasse-fired boilers in a sugar industry plant for researching the tube erosion, convection bank heat transfer, airheater corrosion, secondary air injection for furnace flame manipulation, and ignition stability. Figures 9 and 10 show a typical CFD erosion application in a tube bank for the boiler. Gas velocity contours (a) and trajectories for several particle fractions (b) are shown as per constructed design and modified design (Figs. 9, 10, respectively) [83]. The improvements in boiler tube erosion performance can be deduced by visual assessment alone of the predicted flow and trajectory patterns.

Kær, et al [84–87] carried out CFD modelling of a 33 MW straw-fired boiler incorporating a standalone bed model and a commercial CFD code for gas-space computation. Figures 11, 12 and 13 show the predicted deposition mass flux of the first simulation, the boundary layer controlled deposition and the vapour deposition. The author concluded that poor mixing in the furnace is a key issue leading to high emission levels and relatively high amounts of unburnt carbon in the fly ash. The model was found to correctly predict operational trends same to the boiler experiment. As concluding remark in the future, a significant effort may be put into further improvements and validation of the modelling concept especially with respect to the deposition velocity concept and the tube bank model.

The co-firing of coal and biomass has been recommended for last few years as being advantageous on both an environmental and economic basis along with employability of local farmers providing biomass fuel and thus helping in sustainable development. The co-combustion of biomass as a minor component presents an intermediate situation with a

Table 2 CFD applications in biomass co-firing

Application	Code	Dim	Aim/outcome	Turb. model	Extra model	Agreement with exp.	Authors
Cofiring [93]	Fluent 6.1	3D	To predict the behavior of the biomass in the coal flame	RNG k-ε	P1 FG-biomass	Good	Backreedy, R. I.
Biomass and coal cofired [94]	CINAR	3D	A near approach based on neural networks is proposed	k-ε	Radiation, Lagrangian	NA	Abbas, T.
Co-firing combustors [95]	Fluent UDF code		To develop a fragmentation subroutine applicable to Fluent via a UDF	NA	Lagrangian; Fragmentation model	Reasonable	Syred, N.
Cocombustion boilers [96]	Fluent 6.1 MAT LAB	3D	To optimize burner operation in conventional pulverized-coal-fired boilers	Std k-ε	DOM	NA	Tan, C. K.
Biomass utility boiler [97]	Fluent 5.6	3D	To examine the impact of the large aspect ratio of biomass particles on carbon burnout in cofiring switchgrass/coal	Std k-ε	Lagrangian DOM	NA	Gera, D.
Biomass and coal cofired [98]	Fluent 6.2	3D	To compare bed temperatures in case of coal firing with that of co-firing	Std k-ε	Lagrangian DOM	Fair	Kumar, H.

Dim dimension, *Turb* turbulence, *Std* standard, *DOM* discrete ordinates model (radiation), *P1* P1 radiation model, *Exp* experiment

high reactivity solid. There are a number of commercially available CFD models, and the suitability of the submodels available for biomass combustion is a key factor in selecting an appropriate code. Table 2 summarizes the recent CFD applications in biomass co-firing. Backreedy, et al [93] carried out a CFD modelling study to examine the co-firing of coal and biomass with particular regard to the burnout of the larger diameter biomass particles. The effects of the wood particle size and shape on the burnout of the combined wood and coal char were investigated. The effect of varying the devolatilization and char combustion rate constants for the biomass component in the blend was also investigated. Figure 14 shows the biomass particle traces in the coal-biomass combustion case [93].

Table 2 shows the lift to the recent studies of CFD applications in biomass co-firing. The submodels used in these examples are summarized in the table.

In case of biomass combustion studies there is considerable interest in NO_x formation and unburned carbon in ash. The literatures [99–105] described the biomass combustion and NO_x formation in detail. Ma, et al [99] performed CFD application in a 1 MW industrial wood test furnace coupled with the potassium release and NO_x formation model. The potassium release during biomass combustion is still a subject of current investigation. Ma, et al assume that the biomass potassium release during devolatilization rapidly forms KOH. Figure 15 shows the predicted contours of potassium concentration in the vertical symmetric plane of the furnace. Both the HCN and the NH_3 route have been considered for the NO_x formation and Fig. 16 shows the predicted NO concentrations through NH_3 route. The particle tracks and

temperature distribution are also studied in this work. Good agreement between the predicted and the measured furnace temperature and concentrations of CO_2 and NO_x has been achieved. Table 3 summarizes the recent CFD applications in the NO_x emission modelling. The submodels used in these examples are summarized in the table.

Ravelli, et al [106] and Mueller, et al [107] have used CFD to formulate numerical model of peat-forest residue, Refused derived fuel (RDF) respectively in bubbling fluidized bed combustors. Ravelli, et al [106] compared the devolatilization and the char burnout profiles at the entry ports level, which showed that devolatilization was starting after short time when the fuel was injected. The RDF due to its high intrinsic reactivity favor the fast activation of the homogeneous combustion of volatiles (Fig. 17a). Fuel particles are expected to be broken into small fragments immediately after feeding: since a small particle is burnt faster than a big one, this would accelerate the emission of volatile from RDF. Fixed carbon combustion begins after devolatilization and takes place in different freeboard zones by varying the furnace operating conditions.

Figure 17b shows that devolatilization takes place in the region close to the furnace exit while it is confined to the area just above the bed. Consequently, in the first case, a low percentage of the fuel can be entrained to the furnace exit before the oxidation process is completed. The two cases of low load and high load in commercial combustor have been shown in picture. The study shows that devolatilization depends on fragile structure, intrinsic reactivity, size, temperature and density of properties of particles. If the particles are less fragile, intrinsic reactivity

(a)   **(b)**
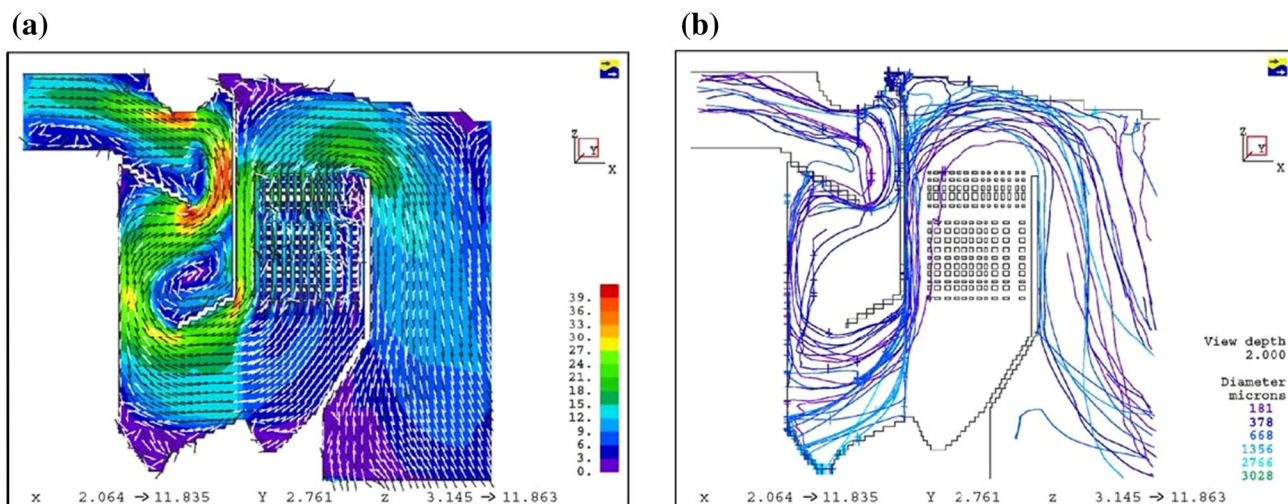
Fig. 9 Flow simulations for the as-constructed design: **a** gas velocity, **b** particle trajectory

(a)   **(b)**
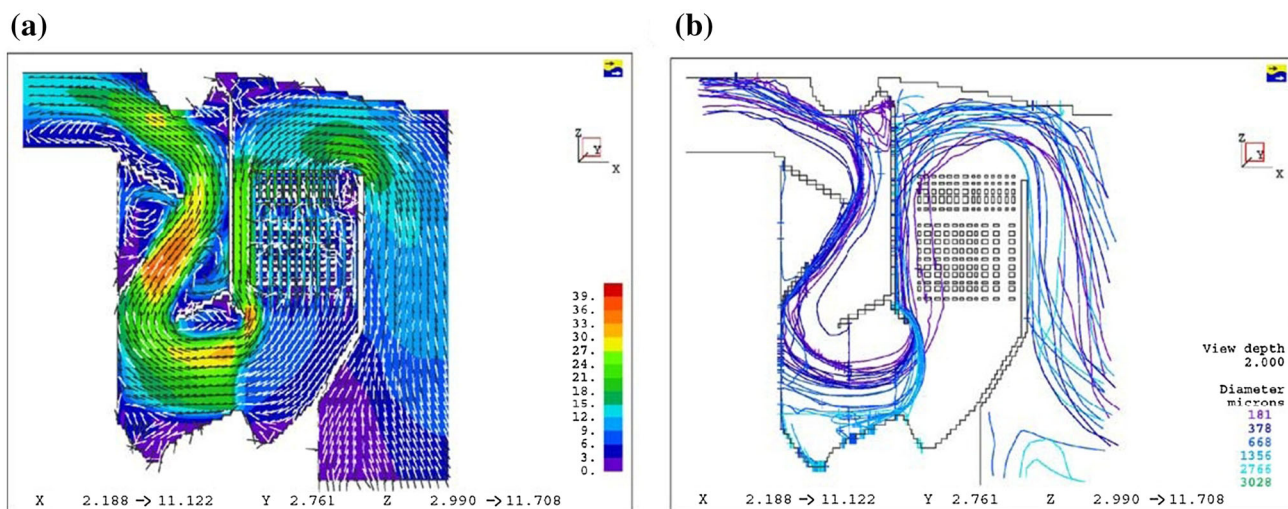
Fig. 10 Flow simulations for the modified design: **a** gas velocity, **b** particle trajectory
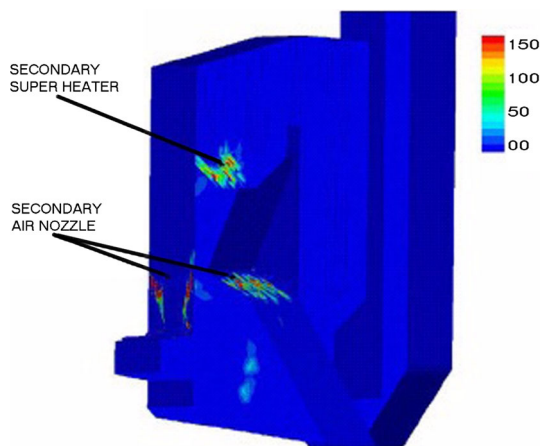
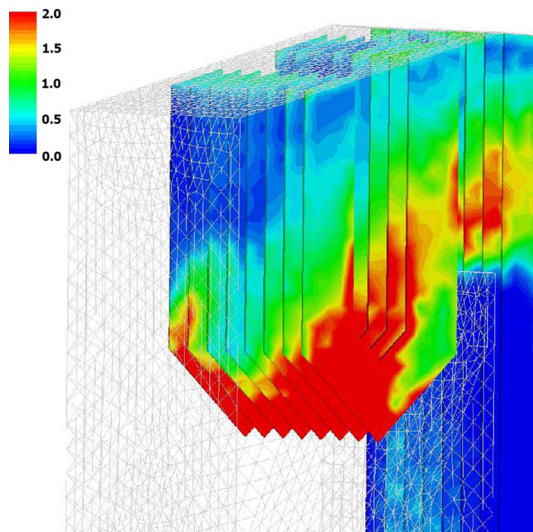Fig. 11 Predicted deposition mass flux in $\mathrm{gm^{-2}h^{-1}}$

is low, size is large and denser then the chances of char devolatilization occurs in bed or during flight from fuel chutes as shown in Fig. 17b.

The devolatilized fuel known as char burns slowly and it takes time depending upon its reactivity and size to burn completely. There is chance that some of the particles may remain unburnt. The char oxidation and char burn out profiles are difficult to study in dense bed due to computational limitations and due surrounding of char particle by sand particle. With present computational approach it is easier to study char oxidation in freeboard region of commercial as well lab scale units with discrete particle model Lagrangian approach. The char burn out is difficult to validate in real combustors and it is not validated in any of studies. In most of studies the aim is not to study the charburn out rather to
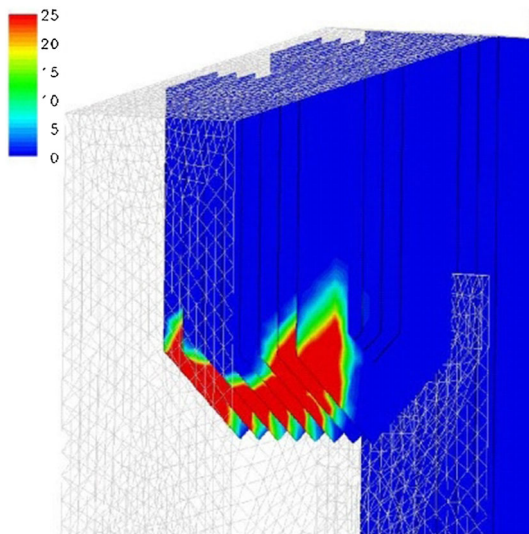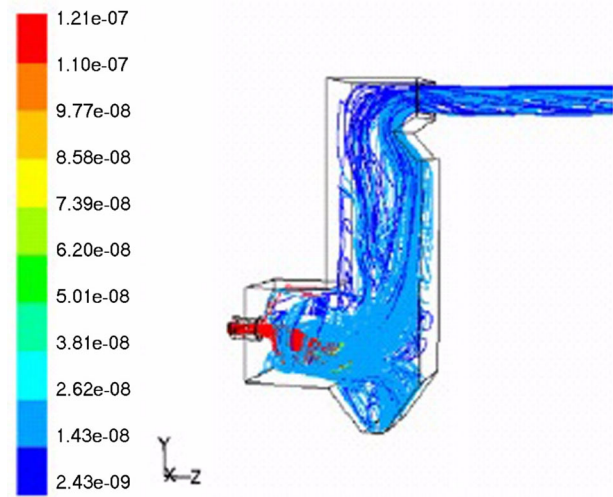
Fig. 12 Close-up of the secondary super heater showing boundary layer controlled deposition flux in $gm^{-2}h^{-1}$ biomass

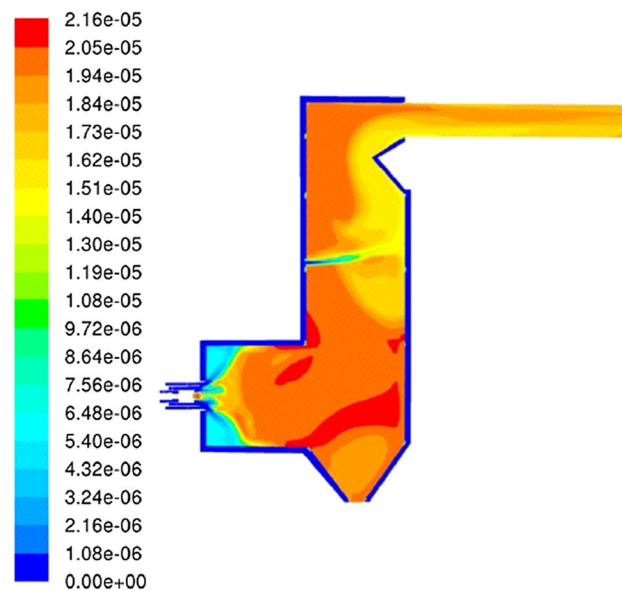**Fig. 13** Close-up of the secondary super heater showing vapour deposition flux in $gm^{-2}h^{-1}$

Fig. 14 Predicted particle traces coloured by particle mass, kg

Fig. 15 Predicted contours of potassium concentration (mol/mol)

validate the CFD model. The char oxidation of RDF fuel in commercial combustor is shown in Fig. 18. It shows that char combustion takes place in the region close to the furnace exit in case of minimum load, while in case maximum load it is confined to the area just above the bed.

Consequently, in the first case, a low percentage of the fuel can be entrained to the furnace exit before the oxidation process is completed. In the minimum load condition, the temperature of the flue gas coming from the bed (971.2 K) is not high enough to rapidly ignite combustion thus fuel particles may be elutriated from the furnace, reducing its efficiency. On the contrary, in maximum load, the temperature of the flue gas coming from the bed (1078.5 K) causes all the fuel to be burnt. For the light

weight particles like rice husk [108] the char oxidation and combustion will take place during trajectory for the case of rice husk as shown in Figs. 19a, b.

Kumar, et al [109] also investigated particle residence time for both biomass and coal for a 45TPH capacity industrial furnace working on co-combustion of biomass and coal. The trajectories were plotted by selecting a desired number of streams for presentation. Discrete phase modelling approach was used to track the fuel particles and to obtain the average residence time in the free-board. As coal and biomass was having different inlet streams with underfeed and overfeed supplies, respectively, there was an inevitable difference in the average residence time of fuel particles, which was expected to be lower for biomass than for coal 5.41 and 8.89 s, respectively as shown in Figs. 20a, b.

466

J. Inst. Eng. India Ser. C (August 2018) 99(4):449–474
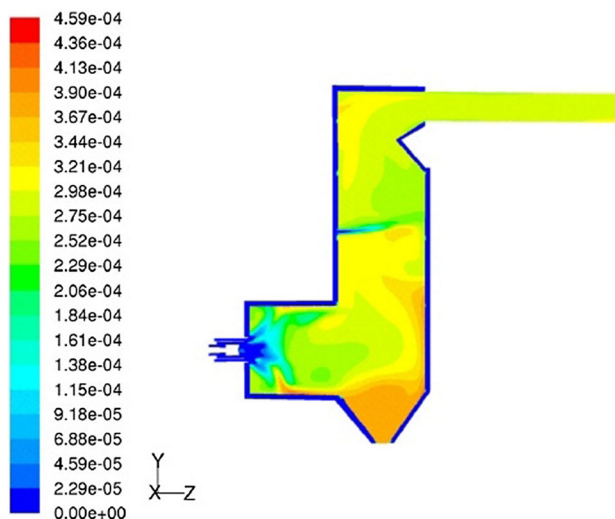
**Fig. 16** Predicted NO formation in the furnace through the NH3 route (mol/mol)

Recent Trends: CFD Applications in Oxy Fuel Combustion

In order to adopt the continuous use of coal, as a cheap and reliable energy source in the future, several advanced combustion technologies have been recently developed. Pre-combustion capture, post-combustion capture, and oxy-fuel combustion are being considered the most efficient utilisation technologies to reduce CO_2, NO_x, and SO_x emissions and fuel consumption [110–112]. However, oxy-fuel (O_2/CO_2) combustion technology has been widely considered the most viable approach amongst the earlier-mentioned technologies in the coal power generations. The fundamental concept of the O_2/CO_2 technology is to use pure oxygen (approximately 95 vol% O_2), producing in air separation units, instead of air (O_2/N_2) in conventional combustion to burn fuel. Due to this high purity of O_2, a very high combustion temperature is achieved in combustion zone; no nitrogen is introduced in this combustion process. This elevated temperature can be diluted by recycling part of flue gas (about 60%) to the combustion chamber in order to reduce the radiation heat transfer to the furnace wall. At the end of this combustion process, the concentration (partial pressure) of carbon dioxide in the exhaust gas is highly increased, and thereby the capturing process of CO_2 becomes easier and economical as compared to that in the air-fired. Also, NO_x and SO_x are decreased, and a high char burnout is achieved in the exit flue gas [113–115]. However, when the oxy-fuel combustion technique was commenced in the last decade, much research was implemented in terms of experimental [114, 116–119] and theoretical studies [120–123], using different scales of furnaces. The main aspects of the

Table 3 CFD applications in NO_x formation of biomass thermochemical conversion

Application	Code	Dim	Aim/Outcome	turb. model	Extra model	Agreement with exp.	Authors
Test furnace [99]	Code	3D	Particle tracks, temperature contours, NO formation, potassium concentration	Std k-ε	Lagrangian; P1; radiation; NO_x formation; potassium release;	Good	Ma, L.
Combustion chamber [100]	Fluent 5.5	3D	Prediction of gaseous emission	SST k-ω	Lagrangian; DTRM; NO_x model	Good	Miltner, M.
Pilot downfired Combustor [101]	Fluent 5	3D	To describe the processes occurring within the gaseous phase of the kiln and of the post combustion chamber	k-ε	P1, Lagrangian; NO_x module	Reasonable	Xiu, S. N.
Fluidized beds [102]	Fluent 6.2	3D	To compare the performance of five global ammonia chemistry mechanisms in full-scale boiler CFD modelling	Std k-ε	DOM; Global ammonia chemistry mechanisms	Well under special conditions	Saario, A.
Biomass combustion [103]	Code	2D	Comparisons of the validity of different simplified NH3-oxidation for mechanisms combustion of biomass	NA	Ammonia oxidation mechanisms	NA	Norstrom, T.
Wood stove [104]	Spider	2D	To model nitric-oxide formation from fuel-bound nitrogen in biomass turbulent non-premixed flames	Std k-ε	DTRM	NA	Weydahl, T.
Bagasse fired boiler [105]	Code	3D	To apply conditional moment closure (CMC) in a bagasse-fired boiler model to obtain predictions of CO and NO in the flue gas.	Std k-ε	Lagrangian; DTRM; PDF; conditional	Reasonable moment closure equation	Rogerson, J. W.
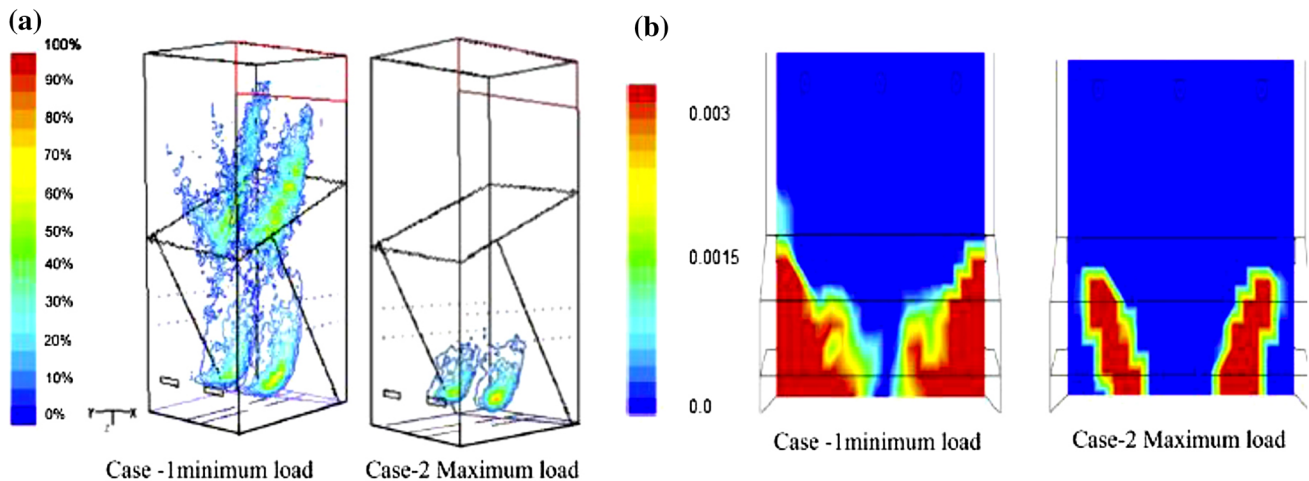
Fig. 17 **a** Fractions of DPM devolatilizations, **b** devolatilization of peat and forest residue
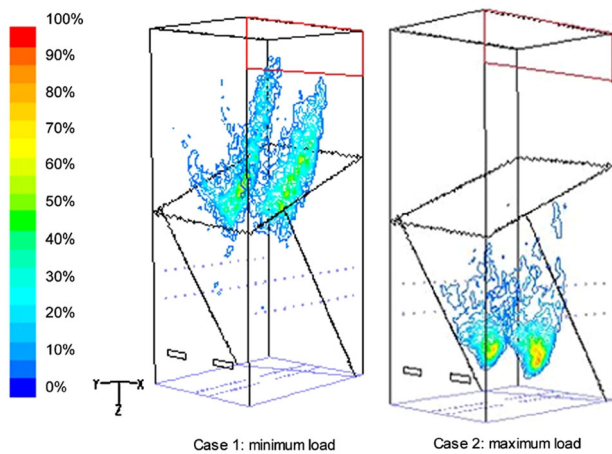
Fig. 18 Fractions of DPM burnout

research were focusing on the species concentrations, flame temperature levels, char burnout, NO_x and SO_x formation, and heat transfer on the furnace wall.

Al-Abbas, et al [124] investigated the coal combustion in 550 MW utility boiler under air-fired and three oxy-fuel-fired scenarios referred as OF25 (25 vol% O_2), OF27 (27 vol% O_2), and OF29 (29 vol% O_2). User-defined functions (UDFs) were written and incorporated into the CFD code to calculate the following mathematical models: the devolatilization, char burnout, multi-step chemical reactions, mass and heat transfer, carbon in flyash, and NO_x formation/destruction. In Fig. 21, the distributions of flue gas temperatures are presented along the height of the furnace at the mid cut of X–Z plane for the air-fired, OF25, OF27, and OF29 combustion cases.

The inlet flow temperatures of gases in the secondary air flow and in the burner gas flows were 473 and 397 K, respectively. Once the reaction processes between coal and oxidizer gases got started the flame temperature is progressively increased to a peak value in the furnace zone as

follows: 1864.37 K for air-fired, 1752.0 K for OF25, 1813.3 K for OF27, and 1865.0 K for OF29. It is clearly seen that a reduction in the levels of the gas temperature when the N_2 is replaced by the CO_2 in the secondary air ducts, particularly in the OF25 and OF27 cases examined. That obvious decrease in the gas temperature was mainly due to the higher volumetric heat capacity of CO_2 compared to N_2 in the gas mixture. On the other hand, the maximum gas temperatures between air fired and OF29 combustion cases were approximately identical. That improvement on the gas temperature of the latter oxy-fuel case was because of increasing O_2 concentration in the feed oxidizer gases.

The distributions of oxygen mass fraction (kg/kg) along the height of the hopper and furnace zone at the mid cut of X–Z plane for all cases examined are shown in Fig. 22. The O_2 distributions were relatively different at all cases investigated. The differences were mainly created in accordance with the O_2 concentrations injected in both the burner ducts and secondary air ducts. It was found that the highest values of O_2 concentrations were observed in the vicinity of the burners region; while the lowest values were predicted in the top and bottom side of the furnace, the region of the higher flame temperatures (Fig. 21). It is interesting to note that for the air-fired case, the higher O_2 concentrations were predicted in the hopper region compared to the oxy-fuel cases. This can be attributed to ignoring the air-leakage in that region. The sequence increase in the gas temperatures of the OF25, OF27, and OF29 cases were strongly coupled with the O_2 concentrations used in the secondary air ducts, which are equal to 25, 27 and 29 vol% O_2, respectively.

Nikolopoulos, et al [125] performed a three dimensional numerical investigation of a large scale boiler under air, partial and full oxy-fuel conditions using ECO-Scrub technology. The ECO-Scrub combustion concept was developed
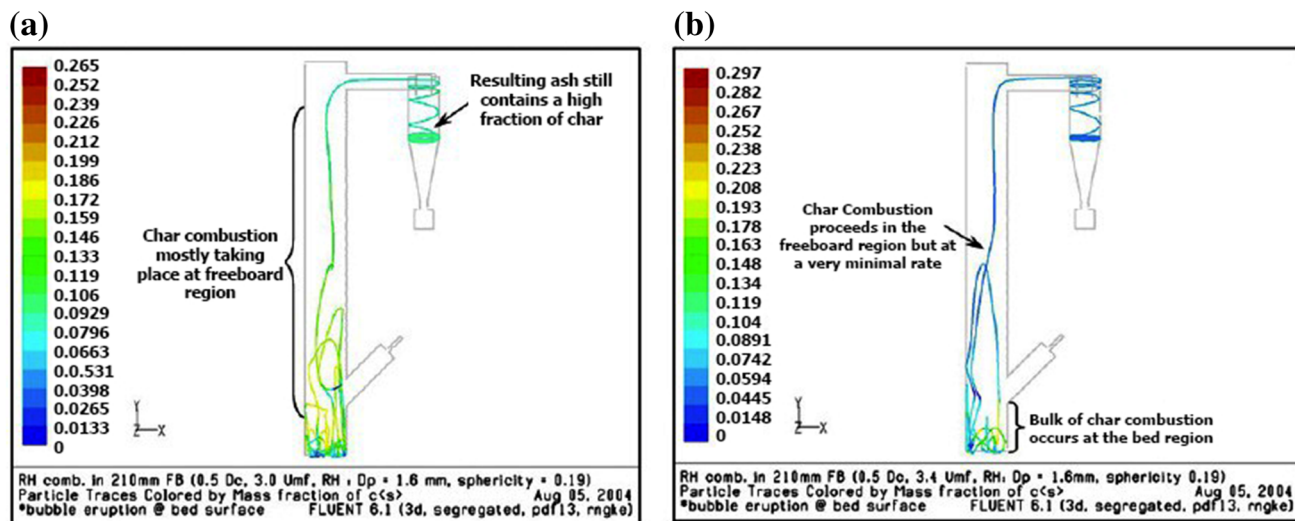
(a)

(b)

Fig. 19 Char fraction of a burning rice husk particle in **a** Model III (one of cases), **b** Model IV
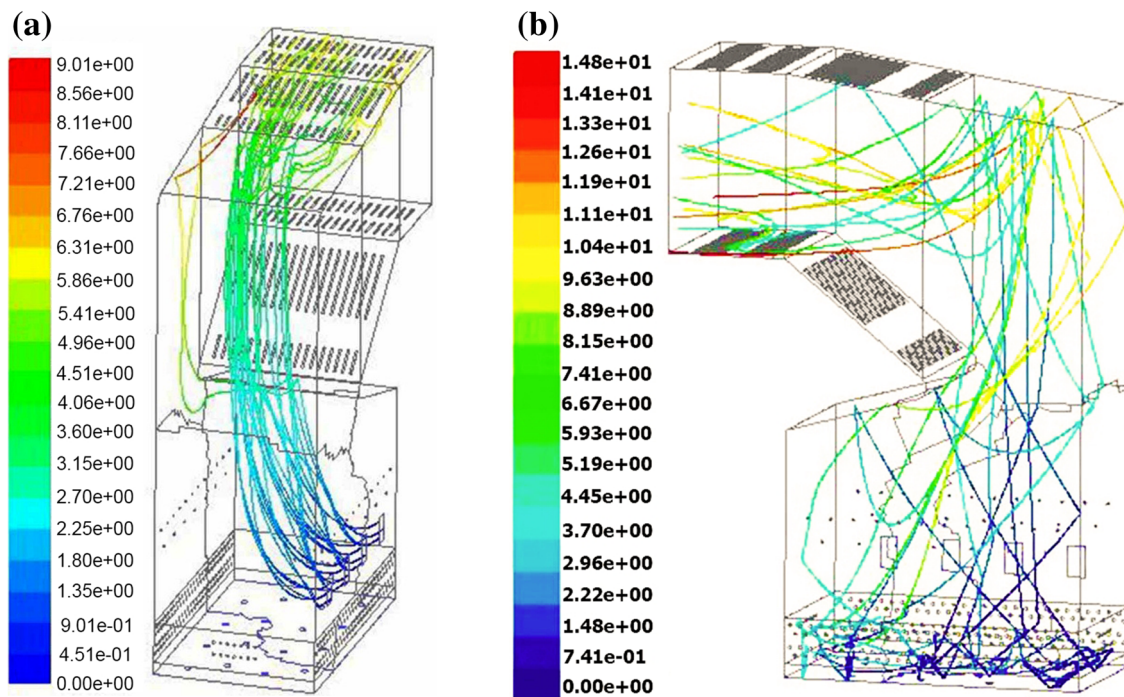
(a)

(b)

Fig. 20 Particle traces coloured by residence time(s) for **a** biomass, **b** coal

specifically for retrofitting applications, for example, for power plants that were not initially designed for carbon capture techniques. The main idea behind the ECO-Scrub concept is the combination of two fundamental CO_2 capture technologies: the partial oxy-fuel mode in the furnace and the post-combustion solvent scrubbing [126]. CO_2 is then removed by a conventional amine scrubbing system, but with lower solvents loading requirements due to the increased CO_2 partial pressure in flue gases. The CO_2 could soon be scrubbed out of the flue gas using a scrubber with monoethanolamine or

similar solvents. The relatively low CO_2 concentration of only 15 vol% in the wet flue gas means that this involves considerable energy input. As the largest portion of the remaining flue gas components consists of the atmospheric nitrogen introduced into the process with the combustion air, holding back this nitrogen before combustion ensures a significant increase in the CO_2 concentration. This is why the concept underlying the oxy-fuel process is to extract the nitrogen from the combustion air prior to combustion by means of an air separation unit (ASU), which means that virtually pure
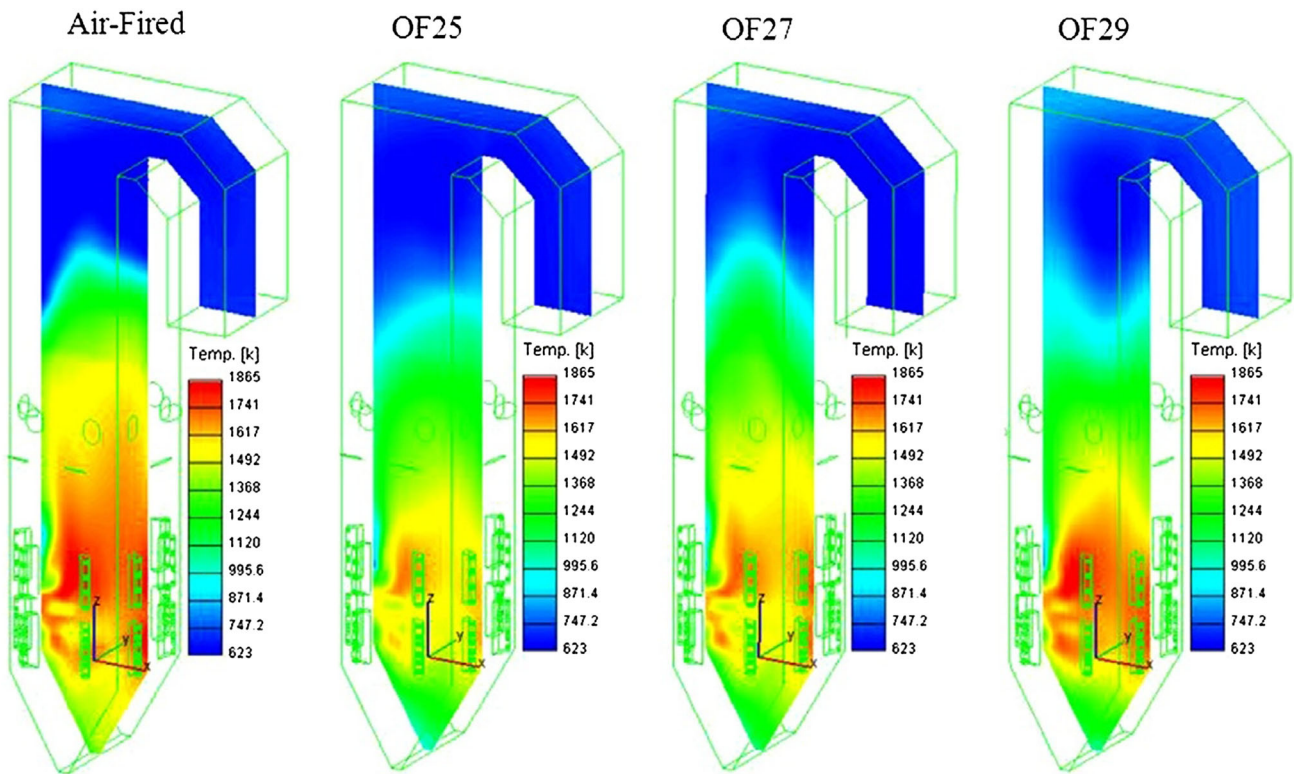
Fig. 21 Distributions of the flue gas temperature (K) along the height of the furnace at the mid cut (X–Z plane) for air-fired, OF25, OF27, and OF29 combustion cases
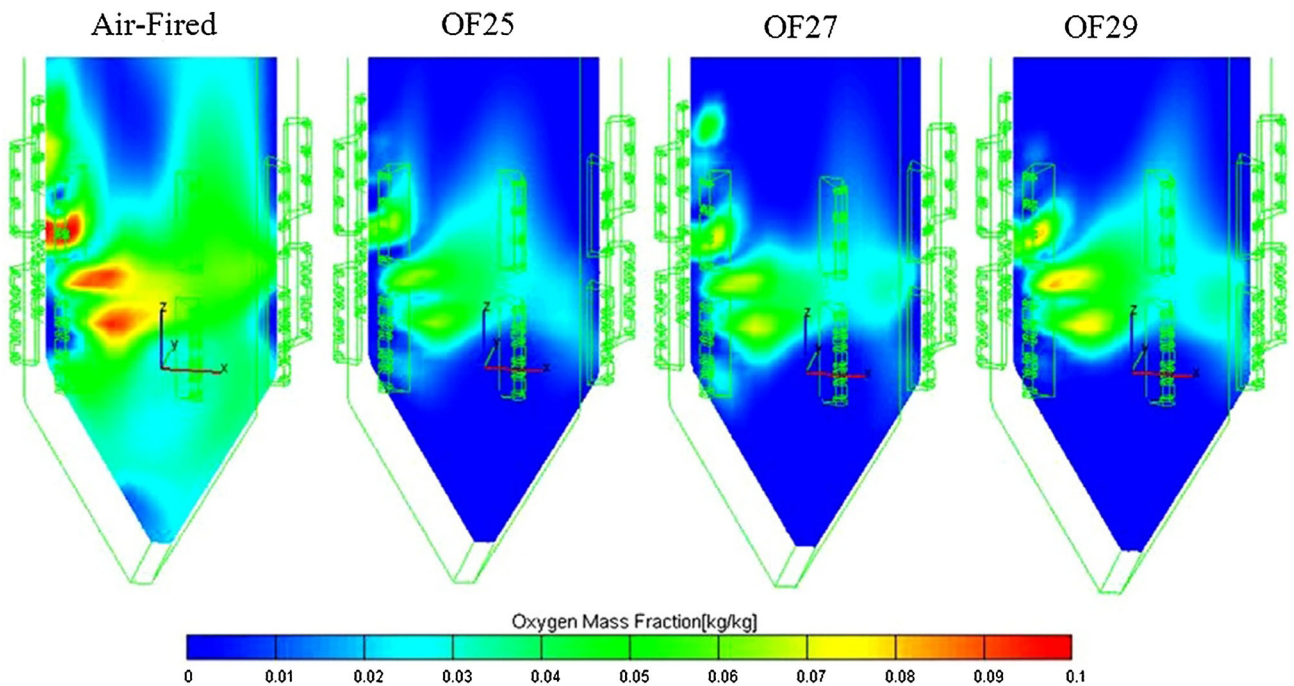
Fig. 22 Distributions of oxygen mass fraction (kg/kg) along the height of the hopper and furnace zone at the mid cut for all cases examined

oxygen is fed to the combustion process. The fundamental principle of the oxy-fuel process is shown in a greatly simplified form in Fig. 23.

Al-Abbas and Naser [127] used a hybrid unstructured grid computational fluid dynamics (CFD) code to model and analyze: an air-fired, oxy-fuel OF25 (25 vol% O_2
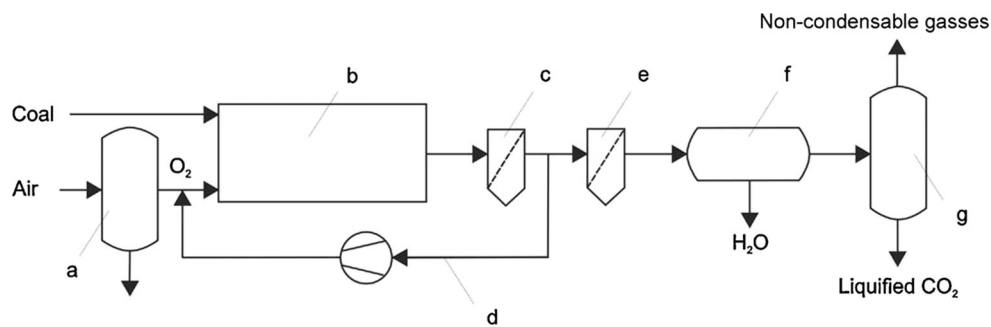
Fig. 23 Fundamental principle of the oxy-fuel process (a: air separation unit; b: furnace and heat transfer sections, that is, boiler; c and e: flue gas cleaning; d: flue gas recycle; f: condenser; g: CO_2 compression and purification)

concentration), oxy-fuel OF27 (27 vol% O_2 concentration), and oxy-fuel OF29 (29 vol% O_2 concentration). The appropriate mathematical models with the related kinetics parameters were implemented to calculate the temperature distributions, species concentrations (O_2, CO_2, CO, H_2O, and H_2), NO_x emission concentrations, and the radiation heat transfer. The multistep chemical reaction mechanisms were conducted on the gas phase and solid phase of coal reaction in one, two, and three-step reaction schemes. The results showed reasonably good agreement against the measured data for all combustion cases; however, in the three-step scheme, the results were highly improved, particularly in the flame envelope zone. For the NO_x calculations, the obvious differences between the air-fired and oxy-fuel (OF27 and OF29) cases were evident. In the OF27 and OF29 cases, the expected increase in the flame temperatures and CO_2 and H_2O concentrations led to a slight increase in the radiative heat fluxes on the furnace wall, with respect to the air-fired case.

Kass, et al [128] have investigated the combustion of Lusatian dried lignite and Polish hard coal in a 0.5 MWth test facility. Pure oxygen (99.95 vol%) was supplied by a tank and mixed with hot flue gas in order to reach oxygen concentrations similarly to the atmospheric air. The effects of excess air and oxygen distribution between primary and secondary air on the maximization of CO_2 concentration in the flue gas as well as the minimization of gaseous pollutants (NO, CO, SO_2) were also found by Kass, et al. To achieve higher CO_2 levels (in the range of 92.15 vol%), excess air should correspond to an oxygen mole fraction of 3.24%. It was also found that NO_x and SO_x emissions increased by increasing excess air. Staged combustion like lower oxygen content in the primary air as compared to secondary air, was also responsible for lesser pollutant emissions.

Vascellari and Cau [129] performed 2D CFD investigations of a 2.4 MW furnace operating under two oxy-fuel combustion mode. Although the oxygen concentration was constant with respect to the reference, air-combustion case, two different oxy-fuel modes were examined: in the first,

constant secondary molar flow rate was undertaken (21% O_2 and 79% CO_2 by volume), while in the second examined case, a constant secondary mass flow was maintained (30% O_2 and 70% CO_2 by volume). In the first case, the velocity field remains relatively unchanged compared to air combustion. However, temperature drop was observed because of the higher specific heat capacity of CO_2 compared to N_2. Burnout remains at the same level as the air combustion, due to both the strong recirculation fields and the char reaction with CO_2.

Several experiments were conducted at 0.3 MW test facility of the CANMET energy (Canadian leader in clean energy research and technology development) using various mixtures of O_2 and CO_2, with oxygen mole fractions in the range of 21–42% [130, 131]. High CO_2 levels, close to the theoretical value of 92, were achieved. Flame temperature was found to increase along with oxygen; O_2 mole fractions of 35% achieved similar temperatures compared to air combustion. NO_x emissions reduced compared to air-firing depending on oxygen concentration and the presence of recycled flue gas. CO emissions do not deviate much from the reference cases and decrease with oxygen concentration, although the decrease rate along the flame is slower compared to air combustion [120, 132].

Hjarstman, et al [114] examined the influence of the flue gas recycle rate, which affects the O_2 fraction entering the furnace, in a 100 kW test unit. Three lignite-fired oxy-fuel flames were investigated (25, 27 and 29 vol% O_2) under a constant stoichiometric ratio. Flame structure and gas concentrations for the oxy-fuel (OF) 25% case were similar to air-firing, while the reduced recycled rates corresponded to higher peak temperatures, lower gas velocities and faster gas burnout. CO levels in the furnace can reach locally high values for the OF 27 and 29 cases; however in the flue gas exiting the boiler, the mole fraction is lower than the air-firing case. NO_x concentration in the exit is decreased by 30% for all oxy-fuel cases. Similar results have been reached by Tan, et al [133] for a 0.3 MW boiler. Profiles of temperature and in-furnace heat transfer can match air-firing through O_2/RFG reduction, while there is significant

J. Inst. Eng. India Ser. C (August 2018) 99(4):449–474

471

potential for NO_x reduction which can be maximized by the appropriate design.

Erfurth, et al [134] performed CFD simulations for a 1200 MW boiler with swirl burners. Several oxy-fuel scenarios, varying in O_2 mole fraction and whether wet or dry flue gas recycle is used, were investigated. Radiation modelling was based on the greyband version of the exponential wide band model (EWBM). In-furnace temperatures dropped when O_2 was 21 vol%. Similar flame behaviour was reached by increasing the O_2 to 27% (wet) or 30% (dry), in order to maintain the same flame temperature. Increased wall heat fluxes occur during oxy-fuel combustion. For the OXY30 dry case, both gas temperature and enthalpy flow at the furnace exit are comparable to air-firing. Although the gas outlet composition is different, no significant changes are expected in the convective part of the boiler and a retrofit appears to be feasible. Finally, for high CO_2 and H_2O mole fractions, the contribution of the gasification reactions to the char burnout increased, while furnace exit temperature remained below the air-fired one for all examined cases.

Liu, et al [135] experimentally investigated the pulverized coal combustion in a 20 kW down-fired combustor for air and various mixtures of O_2/CO_2. Oxy-fuel combustion at O_2 levels comparable to air was found to result in significant temperature decreases and char burnouts, which may lead to destabilization of the flame. The increase of the O_2 to 30% vol results in a temperature profile similar to air combustion, while coal burnout is improved. NO_x and CO levels are high in the main combustion zone, within the vicinity of the combusting coal particles. With higher background fractions of NO_x, more NO_x formed from char combustion can be reduced on the char surface and in the gas phase and thus, the overall NO_x mole fraction decreases compared to air firing. Air staging retains its significant NO_x reduction potential in the oxy-fuel combustion.

Challenges

Challenges Faced during Model Generation

As discussed earlier fluidized bed combustion process is a complex phenomenon due to various chemical and physical reactions taking place inside the furnace. Large scale fluidized bed combustors also incorporate a number of components with varying cross sections and profiles like In-bed superheater, primary and secondary superheaters, convection bank tubes and water walls etc. The 3D model generation considering all these components and intricacies is always a challenging job. Various options using sizing functions for the selection of appropriate mesh elements (hexahedral, tetrahedral, and quadrilateral) required to be explored. In large industrial furnaces it becomes difficult to perform grid independence test in the absence of sufficient data required to optimize the grid generated for the domain of interest.

Challenges Faced during Analysis

The FBC boiler consists of different materials like bed material (sand or refractory), fuel, ash, char and air which makes the selection of input parameters required to run CFD models a difficult job. The high variability found in the heat content of fuel while using it in mixed form, the air constraints imposed during combustion in the fluidized bed and problem of slag clustering evolves various challenges in numerical simulation of real plant furnaces. CFD research was found missing in prediction of characteristics of biomass like particle size, density, porosity and fragmentation. Problem of soot deposition on superheater tubes which has large impact on heat dissipation rate from flue gases to saturated steam and thus overall efficiency of plant lacking in detailed research, because few authors [83–85] have developed UDF to predict soot deposition in real plant combustors, however these models should be available at the back end of the CFD codes for a user friendly approach. Besides it, char inventory is such another problem which needs to be explored under the scope of CFD.

Conclusion

This paper summarized the CFD applications in the field of fluidized bed combustion derived by biomass and co-firing along with latest developments in the field of carbon capture techniques keeping in mind the environmental challenges and sustainable development. CFD codes provided successful information about the temperature distributions, heat flux, species concentrations, NO_x and SO_x emissions, char-burnout, devolatilization during combustion. These parameters play major role in deciding the performance and design considerations of boilers. Simulation results based on CFD codes are proved to be satisfactory having good agreement with experimental data in most of the cases. CFD techniques also proved their potential to analyze and optimize the performance of large industrial furnaces in some cases, especially in the regions where measurements were either difficult or impossible to obtain. However few limitations were observed during running the simulations of 3D problems over full scale furnaces using affordable computers and implementation of combustion models on large scale furnaces fed by a non-conventional fuel. Finally as concluding remarks it can be said that inspite of few limitations of CFD techniques, their application in the field of fluidized bed combustion will widely spread in coming times under the advent of high technology computers and development of chemical and physical models.

472

J. Inst. Eng. India Ser. C (August 2018) 99(4):449–474

References

1. International Energy Agency, Annual Report on Power Generation from Coal—Ongoing Developments and Outlooks (France, 2011)
2. European Union, Directive 2001/80/EC on the limitation of emissions of certain pollutants into the air from large combustion plants. Off. J. Eur. Commun. L **309**, 1–2 (2001)
3. S. Van Loo, J. Koppejan (eds.), *The handbook of biomass combustion and co-firing* (Earthscan, London, 2008)
4. S.R. Gubba, D.B. Ingham, K.J. Larsen, L. Ma, M. Pourkashanian, H.Z. Tan, A. Williams, H. Zhou, Numerical modelling of the co-firing of pulverised coal and straw in a 300 MWe tangentially fired boiler. Fuel Proc. Technol. **104**, 181–188 (2012)
5. Report on biomass co-firing: A Renewable alternative for Utilities (Department of Energy, National Renewable Energy Laboratory, US, 2000).
6. K.V. Narayanan, E. Natarajan, Experimental studies on cofiring of coal and biomass blends in India. Renew. Energy **32**, 2548–2558 (2007)
7. J.M. Ekmann, J.C. Winslow, S.M. Smouse, M. Ramezan, International survey of co-firing coal with biomass and other wastes. Fuel Process. Technol. **54**, 71–88 (1998)
8. N.S. Harding, B.R. Adams, Biomass as a reburning fuel—a specialized co-firing application. Biomass Bioenergy **19**, 29–45 (2000)
9. M. Sami, K. Annamalai, M. Wooldridge, Co-firing of coal and biomass fuel blends. Prog. Energy Combust. Sci. **27**, 7–23 (2001)
10. G. Skodras, P. Grammelis, Emission monitoring during coal waste wood co-combustion in an industrial steam boiler. Fuel **81**, 547–554 (2002)
11. P. Basu, *Combustion and Gasification in Fluidized Beds* (Taylor & Francis, Boca Raton, 2006)
12. F. Scala, R. Chirone, Fluidized bed combustion of alternative solid fuels. Exp. Therm. Fluid Sci. **28**, 691–699 (2004)
13. D.A. Tillman, Co-firing benefits for coal and biomass. Biomass Bioenergy **19**, 6 (2000)
14. D.A. Tillman, Biomass cofiring: the technology, the experience, the combustion consequences. Biomass Bioenergy **19**, 365–384 (2000)
15. S. Pennisi, J.L. Liow, P.A. Schnieder, CFD model development for sugar mill evaporators, in *Third International Conference on CFD in Minerals and Process Industry* (CSIRO, Melbourne, 2013)
16. C. Ghenai, I. Janajreh, CFD analysis of the effects of co-firing biomass with coal. Energy Convers. Manag. **51**, 694–1701 (2010)
17. U.S. Wankhede, D.D. Adgulkar, CFD Simulations of heat transfer in a bubbling fluidized bed for different materials. Ist International Conference on Emerging Trends in Engineering and Technology (Nagpur, India, 2008), pp. 1094–1098
18. S. Oka, *Fluidized Bed Combustion* (Marcel Dekker, New York, 2004)
19. M. Hupa, Fluidized bed combustion of biomass and waste derived fuels—current status and challenges. in *Proceedings of the Waste to Energy Research and Technology Council*, New York City, 2005
20. S. Bittani, B. Paolo, M.C. Campi, A.D. Marco, G. Poncia, W. Prandoni, A model of a bubbling fluidized bed combustor oriented to char mass estimation. IEEE Trans. Control Syst. Technol. **8**, 247–258 (2000)
21. M. Leva, *Fluidization* (McGraw-Hill, New York, 1959)
22. J.F. Davidson, D. Harrison, *Fluidized Particles* (Cambridge University Press, New York, 1963)
23. R. Toomey, H.F. Johnstone, Gas fluidization of solid particles. Chem. Eng. Prog. **48**, 220–226 (1952)
24. D. Kunii, O. Levenspiel, *Fluidization Engineering*, 2nd edn. (Butterworth-Heinemann, Stoneham, 1991)
25. J. Werther, *Hydrodynamics and Mass Transfer Between the Bubble and Emulsion Phases in Fluidized Beds of Sand and Cracking Catalyst* (Fluidization, Engineering Foundation, New York, 1983)
26. M.M. Avedesian, J.F. Davidson, Combustion of carbon particles in a fluidized bed. Trans. Inst. Chem. Eng. **51**, 121–131 (1973)
27. J. Adanez, J.C. Abanades, L.F. de Diego, Determination of coal combustion reactivities by burnout time measurements in a batch fluidized bed. Fuel **73**, 287–293 (1994)
28. R.D. La Nauze, Coal devolatilization in fluidized-bed combustors. Fuel **61**, 771–774 (1982)
29. I.B. Ross, J.F. Davidson, The combustion of carbon particles in a fluidised bed. Trans. Inst. Chem. Eng. **59**, 108–114 (1981)
30. F. Scala, P. Salatino, Modelling fluidized bed combustion of high volatile solid fuels. Chem. Eng. Sci. **57**, 1175–1196 (2002)
31. W.C. Yang, *Handbook of Fluidization and Fluid Particle Systems* (Marcel Dekker, New York, 2003)
32. C.Y. Wen, Y.W. Yu, Mechanics of fluidization. Eng. Progr. Symp. **162**, 100–125, (1966)
33. K. Kato, C.Y. Wen, Bubble assemblage model for fluidized bed catalytic reactors. Chem. Eng. Sci. **24**, 1351–1369 (1969)
34. A. Galgano, P. Salatino, F. Crescitellis Scale, P.L. Maffettone, A model of the dynamics of a fluidized bed combustor burning bio-mass. Combust. Flame **140**, 371–384 (2005)
35. T. Nussbaumer, in *Energie aus Biomasse* (Springer, Berlin, ISBN 3-540-64853-42001, 288–389, 2001)
36. L.L. Baxter, in *Handbook of Biomass Combustion In addition to Conventional Two-Stage Combustion, Pri and Co-firing* (Twente University Press, ISBN 9036517737, 26, 2002)
37. Ø. Skreiberg, Theoretical and Experimental Studies on Emissions from Wood Combustion. Ph.D. Thesis, Norwegian University, Trondheim, 1997
38. R. Salzmann, T. Nussbaumer, Fuel staging for NOₓ reduction in biomass combustion. Experiments and modeling. Energy Fuels **15**, 575–582 (2001)
39. U. Schnell, Numerical modelling of solid fuel combustion processes using advanced CFD-based simulation tools. Int. J. Prog. Comput. Fluid Dyn. **1**, 208–218 (2001)
40. B. Peters, Numerical Simulation of Packed Bed Combustion, in *Seventh European Conference on Industrial Furnaces and Boilers*, 1–4 April Porto (Portugal), 1–23, 1997
41. C. Bruch, B. Peters, T. Nussbaumer, Modelling wood combustion under fixed bed conditions. Fuel **82**, 729–738 (2003)
42. T. Nussbaumer, Wood combustion. in *Advances in Thermochemical Biomass Conversion* (Blackie Academic and Professional, London, ISBN 0 7514 0171 4, 1994), pp. 575–589
43. T. Nussbaumer, Combustion and co-combustion of biomass: fundamentals, technologies, and primary measures for emission reduction. Energy Fuels **17**, 1510–1521 (2003)
44. C. Hirsch, *Numerical computation of internal and external flows* (Butterworth-Heinemann, Waltham, 2007)
45. S.V. Patankar, *Numerical Heat Transfer and Fluid Flow* (Taylor & Francis, USA, 1980)
46. D. Gera, M. Gautam, Y. Tsuji, T.Tanaka Kawaguchi, Computer simulation of bubbles in large-particle fluidized beds. Powder Technol. **98**, 38–47 (1998)
47. H. Enwald, E. Peirano, A.E. Almstedt, Eulerian two-phase flow theory applied to fluidization. Int. J. Multiph. Flow **22**(1), 21–66 (1966)
48. C.Y. Wen, Y.H. Yu, Mechanics of fluidization. Chem. Eng. Prog. Symp. Ser. **62**, 100–111 (1996)
49. S. Ergun, Fluid flow through packed columns. Chem. Eng. Prog. **48**, 89–94 (1952)
50. D. Gidaspow, R. Bezburuah, J. Ding, Hydrodynamics of circulating fluidized beds, kinetic theory approach, *Fluidization VII Proceedings of the Seventh Engineering Foundation Conference on Fluidization*, Gold Coast (Australia),75–82, 3–8 May 1992

J. Inst. Eng. India Ser. C (August 2018) 99(4):449–474

473

51. C.C. Pain, S. Mansoorzadeh, C.R.E. de Oliveira, A study of bubbling and slugging fluidized bed s using the two-fluid granular temperature model. Int. J. Multiph. Flow **27**, 527–551 (2001)

52. J.A.M. Kuipers, W. Prins, W.P.M. Van Swaaij, Numerical calculation of wall to bed heat transfer coefficients in gas-fluidized beds. AIChE J. **38**, 1079–1091 (1992)

53. A. Schmidt, U. Renz, Eulerian computation of heat transfer. Chem. Eng. Sci. **54**, 5515–5522 (1999)

54. M. Gustavasson, A.E. Almstedt, Numerical simulation of fluid dynamics in fluidized beds with horizontal heat exchanger tubes. Chem. Eng. Sci. **55**, 857–863 (2000)

55. R. Clift, M.E. Weber, J.R. Grace, *Bubbles, Drops, and Particles* (Academic Press, New York, 1978)

56. R.B. Bird, W.E. Stewart, E.N. Lightfoot, *Transport Phenomena* (Wiley, New York, 2002)

57. M. Syamlal, T.J. O'Brien, Computer simulation of bubbles in a fluidized bed. AIChE Symp. Ser. **85**, 22–31 (1989)

58. D. Gidaspow, *Multiphase Flow and Fluidization: Continuum and Kinetic Theory Descriptions* (Academic Press, San Diego, 1994)

59. C.Y. Wen, Y.H. Yu, Mechanics of fluidization. Chem. Eng. Prog. Symp. Ser. **62**, 100–111 (1966)

60. Y. Tsuji, T. Kawagushi, T. Tanaka, Discrete particle simulation of two-dimensional fluidized bed. Powder Technol. **77**, 79–87 (1993)

61. B.P.B. Hoomans, J.A.M. Kuipers, W.J. Briels, W.P.M. Van Swaaij, Discrete particle simulation of bubble and slug formation in a two-dimensional gas-fluidised bed: a hard-sphere approach. Chem. Eng. Sci. **51**, 99–118 (1996)

62. N. Kobayashi, R. Yamazaki, S. Mori, A study on the behavior of bubbles and solids in bubbling fluidized beds. Powder Technol. **113**, 327–344 (2000)

63. Y. Kaneko, T. Shiojima, M. Horio, DEM simulation of fluidized beds for gas-phase olefin polymerization. Chem. Eng. Sci. **54**, 5809–5821 (1999)

64. M.A. Van der Hoef, M. Van Sint Annaland, J.A.M. Kuipers, Computational fluid dynamics for dense gas-solid fluidized beds: a multiscale modeling strategy. Chin. Particuol. **3**, 69–77 (2005)

65. M. Chiesa, V. Mathiesen, J.A. Melheim, B. Halvorsen, Numerical simulation of particulate flow by the Eulerian-Lagrangian and the Eulerian-Eulerian approach with application to a fluidized bed. Comput. Chem. Eng. **29**, 291–304 (2005)

66. S.T. Johansen, H. Laux, Simulations of granular materials flows, in *Proceedings of the International Symposium on the Reliable Flow of Particulate Solids* (Telemark College, Porsgrunn, Norway, 11–13 August 1999)

67. K.W. Morton, D.F. Mayers, *Numerical Solution of Partial Differential Equations: An Introduction* (Cambridge University Press, Cambridge, 1994)

68. H.K. Versteeg, W. Malalasekera, *An Introduction to Computational Fluid Dynamics: The Finite*, vol. Method (Addison-Wesley, Longman, New York, 1995)

69. G. Strang, G. Fix, *An Analysis of the Finite Element Method* (Prentice-Hall, Englewood Cliffs, NJ, 1973)

70. R.H. Gallagher, *Finite Element Analysis: Fundamentals* (Prentice-Hall, Englewood Cliffs, NJ, 1975)

71. C.D. Blasi, Modeling chemical and physical processes of wood and biomass pyrolysis. Progress. Energy Combust. Sci. **34**, 47–90 (2008)

72. B. Moghtaderi, The state-of-the-art in pyrolysis modelling of lignocellulosic solid fuels. Fire Mater. **30**, 1–34 (2006)

73. J.C. Wurzenberger, S. Wallner, H. Raupenstrauch, J.G. Khinast, Thermal conversion of biomass: comprehensive reactor and particle modeling. AIChE J. **48**, 2398–2411 (2002)

74. J. Corella, A. Sanz, Modeling circulating fluidized bed biomass gasifiers. A pseudo-rigorous model for stationary state. Fuel Process. Technol. **86**, 1021–1053 (2005)

75. FLUENT 6.1 user's guide, vol. 1–5, (Lebanon, 2003)

76. H. Kobayashi, J. B. Howard, A. F. Sarofim, Coal devolatilization at high temperatures, in *Proceedings of 16th International Symposium on Combustion*, 1976

77. A.M. Eaton, L.D. Smoot, S.C. Hill, C.N. Eatough, Components, formulations, solutions, evaluation, and application of comprehensive combustion models. Prog. Energy Combust. Sci. **25**, 387–436 (1999)

78. J. Pallares, I. Arauzo, A. Williams, Integration of CFD codes and advanced combustion models for quantitative burnout determination. Fuel **86**, 2283–2290 (2007)

79. C.E.J. Bakul, V.Y. Gershtein, L. Xianming, *Computational Fluid Dynamics in Industrial Combustion* (CRC Press, New York, 2001)

80. B.E. Launder, D.B. Spalding, *Lectures in Mathematical Models of Turbulence* (Academic Press, London, 1972)

81. S.A. Morsi, A.J. Alexander, An investigation of particle trajectories in two-phase flow systems. J. Fluid Mech. **55**, 193–208 (1972)

82. A. Haider, O. Levenspiel, Drag coefficient and terminal velocity of spherical and nonspherical particles. Powder Technol. **58**, 63–70 (1989)

83. T.F. Dixon, A.P. Mann, F. Plaza, W.N. Gilfillan, Development of advanced technology for biomass combustion—CFD as an essential tool. Fuel **84**, 1303–1311 (2005)

84. S.K. Kær, Numerical modelling of a straw-fired grate boiler. Fuel **83**, 1183–1190 (2004)

85. S.K. Kær, L.A. Rosendahl, L.L. Baxter, Towards a CFD-based mechanistic deposit formation model for straw-fired boilers. Fuel **85**, 833–848 (2006)

86. S. K. Kær, L. A. Rosendahl, Extending the modelling capacity of CFD codes applied to biomass-fired boilers, in *Proceedings of ECOS*, Copenhangen, Denmark, 251–264, June 30-July 2, 2003

87. S. K. Kær, L. A. Rosendahl, L. L. Baxter, Extending the capability of CFD codes to assess ash related problems in biomass fired boilers, in *Proceedings of 227th ACS Annual Meeting*, Anaheim California, Division of Fuel Chemistry, No. 12, March 28–April 1, 2004

88. K.S. Shanmukharadhya, Simulation and thermal analysis of the effect of fuel size on combustion in an industrial biomass furnace. Energy Fuels **21**, 1895–1900 (2007)

89. F. Marias, A model of a rotary kiln incinerator including processes occurring within the solid and the gaseous phases. Comput. Chem. Eng. **27**, 813–825 (2003)

90. K.S. Shanmukharadhya, K.G. Sudhakar, Effect of fuel moisture on combustion in a bagasse fired furnace. J. Energy Resour. Technol.-Trans. ASME **129**, 248–253 (2007)

91. C.S.B. Dixit, P.J. Paul, H.S. Mukunda, Part II: computational studies on a pulverised fuel stove. Biomass Bioenergy **30**(7), 684–691 (2006)

92. C.D. Goddard, Y.B. Yang, J. Goodfellow, V.N. Sharifi, J. Swithenbank, J. Chartier, D. Mouquet, R. Kirkman, D. Barlow, S. Moseley, Optimisation study of a large waste-to-energy plant using computational modelling and experimental measurements. J. Energy Inst. **78**(3), 106–116 (2005)

93. R.I. Backreedy, L.M. Fletcher, J. Jones, L. Ma, M. Pourkashanian, A. Williams, Co-firing pulverised coal and biomass: a modeling approach. Proc. Combust. Inst. **30**, 2955–2964 (2005)

94. T. Abbas, M.M. Awais, F.C. Lockwood, An artificial intelligence treatment of devolatilization for pulverized coal and biomss in co-fired flames. Combust. Flame **132**(3), 305–318 (2003)

95. N. Syred, K. Kurniawan, T. Griffths, T. Gralton, R. Ray, Development of fragmentation models for solid fuel combustion and gasification as subroutines for inclusion in CFD codes. Fuel **86**(14), 2221–2231 (2007)

96. C.K. Tan, S.J. Wilcox, J. Ward, Use of artificial intelligence techniques for optimisation of cocombustion of coal with biomass. J. Energy Inst. **79**(1), 19–25 (2006)

474

J. Inst. Eng. India Ser. C (August 2018) 99(4):449–474

97. D. Gera, M.P. Mathur, M.C. Freeman, A. Robinson, Effect of large aspect ratio of biomass particles on carbon burnout in a utility boiler. Energy Fuels **16**(6), 1523–1532 (2002)

98. H. Kumar, S.K. Mohapatra, R.I. Singh, Study of a 30 MW bubbling fluidized bed combustor based on co-firing biomass and coal. Sadhana Acad. Process. Eng. Sci. **40**, 1283–1299 (2015)

99. L. Ma, J.M. Jones, M. Pourkashanian, A. Williams, Modelling the combustion of pulverized biomass in an industrial combustion test furnace. Fuel **86**, 1959–1965 (2007)

100. M. Miltner, A. Miltner, M. Harasek, A. Friedl, Process simulation and CFD calculations for the development of an innovative baled biomass-fired combustion chamber. Appl. Therm. Eng. **27**(7), 1138–1143 (2007)

101. V. Zarnescu, S.V. Pisupati, An integrative approach for combustor design using CFD methods. Energy Fuels **16**(3), 622–633 (2002)

102. A. Saario, A. Oksanen, Comparison of global ammonia chemistry mechanisms in biomass combustion and selective noncatalytic reduction process conditions. Energy Fuels **22**(1), 297–305 (2008)

103. T. Norstrom, P. Kilpinen, A. Brink, E. Vakkilainen, M. Hupa, Comparisons of the validity of different simplified NH3-oxidation mechanisms for combustion of biomass. Energy Fuels **14**(5), 947–952 (2000)

104. T. Weydahl, M. Bugge, I.R. Gran, I.S. Ertesvag, Computational modeling of nitric oxide formation in biomass combustion. Appl. Mech. Eng. **7**, 125–142 (2002)

105. J.W. Rogerson, J.H. Kent, R.W. Bilger, Conditional moment closure in a bagasse-fired boiler. Proc. Combust. Inst. **31**, 2805–2811 (2007)

106. S. Ravelli, A. Perdichizzi, G. Barigozzi, Description, applications and numerical modeling of bubbling fluidized bed combustion in waste-to-energy plants. Prog. Energy Combust. Sci. **34**, 224–253 (2008)

107. C. Mueller, A. Brink, M. Hupa, Numerical simulation of the combustion behavior of different biomasses in a bubbling fluidized bed boiler, in *Proceedings of 18th International Conference on Fluidized Bed Combustion*, Toronto, Ontario, Canada, 2005

108. M. Rozainee, S.P. Ngo, A.A. Salema, K.G. Tan, Computational fluid dynamics modeling of rice husk combustion in a fluidized bed combustor. Powder Technol. **203**, 331–347 (2010)

109. H. Kumar, S.K. Mohapatra, R.I. Singh, Three-dimensional CFD modelling of a fluidised bed combustor fuelled by biomass and coal. Mater. Res. Innov. **19**, 118–124 (2015)

110. A. Doukelis, I. Vorrias, P. Grammelis, E. Kakaras, M. Whitehouse, G. Riley, Partial O_2-fired coal power plant with post-combustion CO_2 capture: a retrofitting option for CO_2 capture ready plants. Fuel **88**, 2428–2436 (2009)

111. M. Kanniche, R. Gros-Bonnivard, P. Jaud, J. Valle-Marcos, J.M. Amann, C. Bouallou, Pre-combustion, post-combustion and oxy-combustion in thermal power plant for CO_2 capture. Appl. Therm. Eng. **30**, 53–62 (2009)

112. T. Wall, Y. Liu, C. Spero, L. Elliott, S. Khare, R. Rathnam, An overview on oxyfuel coal combustion-state of the art research and technology development. Chem. Eng. Res. Des. **87**, 1003–1016 (2009)

113. E. Kakaras, A. Koumanakos, A. Doukelis, D. Giannakopoulos, I. Vorrias, Oxyfuel boiler design in a lignite-fired power plant. Fuel **86**, 2144–2150 (2007)

114. S. Hjärtstam, K. Andersson, F. Johnsson, B. Leckner, Combustion characteristics of lignite-fired oxy-fuel flames. Fuel **88**, 2216–2224 (2009)

115. W. Zhou, D. Moyeda, Process evaluation of oxy-fuel combustion with flue gas recycle in a conventional utility boiler. Energy Fuel **24**, 2162–2169 (2010)

116. K. Andersson, F. Normann, F. Johnsson, B. Leckner, NO emission during oxy-fuel combustion of lignite. Ind. Eng. Chem. Res. **47**, 1835–1845 (2008)

117. C. Sheng, Y. Li, Experimental study of ash formation during pulverized coal combustion in O_2/CO_2 mixtures. Fuel **87**, 1297–1305 (2008)

118. Y. Qiao, L. Zhang, E. Binner, M. Xu, C.Z. Li, An investigation of the causes of the difference in coal particle ignition temperature between combustion in air and in O_2/CO_2. Fuel **89**, 3381–3387 (2010)

119. L. Zhang, E. Binner, Y. Qiao, C.Z. Li, In situ diagnostics of Victorian brown coal combustion in O_2/N_2 and O_2/CO_2 mixtures in drop-tube furnace. Fuel **89**, 2703–2712 (2010)

120. E.H. Chui, M.A. Douglas, Y. Tan, Modeling of oxy-fuel combustion for a western Canadian sub-bituminous coal [small star, filled]. Fuel **82**, 1201–1210 (2003)

121. S.P. Khare, T.F. Wall, A.Z. Farida, Y. Liu, B. Moghtaderi, R.P. Gupta, Factors influencing the ignition of flames from air-fired swirl pf burners retrofitted to oxy-fuel. Fuel **87**, 1042–1049 (2008)

122. F. Normann, K. Andersson, B. Leckner, F. Johnsson, High-temperature reduction of nitrogen oxides in oxy-fuel combustion. Fuel **87**, 3579–3585 (2008)

123. A.H. Al-Abbas, J. Naser, D. Dodds, CFD modelling of air-fired and oxy-fuel combustion of lignite in a 100 KW furnace. Fuel **90**, 1778–1795 (2011)

124. A.H. Al-Abbas, J. Naser, D. Dodds, CFD modelling of air-fired and oxy-fuel combustion in a large-scale furnace at Loy Yang A brown coal power station. Fuel **102**, 646–665 (2012)

125. N. Nikolopoulos, A. Nikolopoulos, E. Karampinis, P. Grammelis, E. Kakaras, Numerical investigation of the oxy-fuel combustion in large scale boilers adopting the ECO-Scrub technology. Fuel **90**, 198–214 (2011)

126. G. Scheffknecht, L. Al-Makhadmeh, U. Schnell, J. Maier, Oxy-fuel coal combustion—a review of the current state-of-the-art. Int. J. Greenh. Gas Control **5S**, S16–S35 (2011)

127. A.H. Al-Abbas, J. Naser, Numerical study of one air-fired and two oxy-fuel combustion cases of propane in a 100 kW furnace. Energy Fuels **26**, 952–967 (2012)

128. H. Kass, S. Tappe, H.J. Krautz, The combustion of dry lignite under oxy-fuel process conditions in a 0.5 MWth test plant. Phys. Proc. **1**, 423–430 (2008)

129. M. Vascellari, G. Cau, Numerical simulation of pulverised coal oxy-combustion with exhaust gas recirculation, in *Fourth International Conference on Clean Coal Technologies*, CCT, 2009

130. E. Croiset, K.V. Thambimuthu, A. Palmer, Coal combustion in O_2/CO_2 mixtures compared with air. Can. J. Chem. Eng. **78**, 402–407 (2000)

131. E. Croiset, K.V. Thambimuthu, NO_x and SO_2 emission from O_2/CO_2 recycled coal combustion. Fuel **80**, 2117–2121 (2001)

132. E. Croiset, K.V. Thambimuthu, *Coal combustion with flue gas recirculation for CO_2 recovery*, in ed. by P. Riemer, B. Eliasson, A. Wokaun Greenhouse Gas Technologies (Amsterdam, 1999), pp. 581–586

133. Y. Tan, E. Croiset, M.A. Douglas, V. Thambimuthu, Combustion characteristics of coal in a mixture of oxygen and recycled flue gas. Fuel **85**, 507–512 (2006)

134. J. Erfurth, D. Toporov, M. Forster, R. Kneer, Numerical simulation of a 1200 MWth pulverized fuel oxy-firing furnace, in *Fourth International Conference on Clean Coal Technologies*, CCT, 2009

135. H. Liu, R. Zailani, B.M. Gibbs, Comparisons of pulverized coal combustion in air and in mixtures of O_2–CO_2. Fuel **84**, 833–840 (2005)